



University of Bremen

Alfred Wegener Institute, Helmholtz Centre for Polar and  
Marine Research

MASTER THESIS

---

# Comparison of the Past Climate in Northern Canada and Greenland

---

*Author:*

Sara Khosravi

*Anagraphic data:*

Tehran (IR), 30.03.1991

*Matriculation Number:*

2995902

*First Supervisor:*

Prof. Dr. Gerrit Lohmann

*Second Supervisor:*

Dr. Martin Werner

*Tutor:*

Dr. Evan Gowan

December 23, 2017



## Declaration of copyright

Hereby I declare that my Masters Thesis was written without external support and that I did not use any other sources and auxiliary means than those quoted. All statements which are literally or analogously taken from other publications have been identified as quotations.

## Declaration with regard to publishing theses

I agree that for research purposes third parties can look into my thesis stored in the University archive.

**Bremen / December 23, 2017**

**Sara Khosravi**





# Abstract

Despite the fact that the Innuitian and Greenland Ice Sheets were close proximity high latitude ice sheets during Last Glacial Maximum (LGM), the Innuitian Ice Sheet retreated to isolated ice caps, while Greenland maintained an ice sheet. The Innuitian Ice Sheet is reconstructed with the ICESHEET program from 30 ka to present time in this thesis. The main goal of this study is to determine surface elevation variation due to changes in ice thickness and glacial isostatic adjustment (GIA). Ice margin, topography, and shear stress are input variables. The Innuitian Ice Sheet margins are reconstructed from 30 ka to maximum extent in 22 ka, while later times use an existing reconstruction. The elevation of the Agassiz Ice Cap decreased by 520 m during the early Holocene retreat from 14 ka to 8 ka. The Devon Ice Cap elevation decreased 540 m dramatically from 13 ka to 12 ka.

To assess the reasons for different retreat of the Innuitian and Greenland Ice Sheets,  $\delta^{18}\text{O}$  of the Agassiz and Devon Ice Caps, which are remnant of the Innuitian Ice Sheet, are used to reconstruct the local temperature in the early Holocene.  $\delta^{18}\text{O}$ , a climate proxy, has linear relation with temperature. This linear relationship is obtained utilizing ECHAM-wiso model and compared to same, obtained by Dansgaard, hereafter referred to as ECHAM temperature relation and Dansgaard temperature relation, respectively. Moreover, the relation between  $\delta^{18}\text{O}$  and elevation is calculated from Dansgaard temperature relation based on lapse rate and is compared to relation between  $\delta^{18}\text{O}$  and elevation using ECHAM-wiso model, here referred to as Dansgaard elevation relation and ECHAM elevation relation, respectively. The reconstructed elevation change is used to correct  $\delta^{18}\text{O}$ . Both of the ice cores have reliable  $\delta^{18}\text{O}$  records between present to 11700 years age. The Devon Ice

cap has constant elevation from 12 ka to present time, while the Agassiz elevation decreases 408 m from 12 ka to present time, which increases  $\delta^{18}\text{O}$  by 2.46 ‰ and 1.32 ‰ using the ECHAM and Dansgaard elevation relations, respectively. The correspond temperature rise using ECHAM temperature relation is 3.64 °C and using Dansgaard temperature relation is 2.14 °C.

The North Greenland Ice Core Project (NGRIP) core has been chosen to represent Greenland. The change of NGRIP elevation through the Holocene is obtained by assuming homogeneous climate in this region during the Holocene and using the difference of  $\delta^{18}\text{O}$  between the Agassiz Ice Cap and NGRIP. The elevation change of NGRIP is 422 m and 226 m relative to present time using the Dansgaard and ECHAM elevation relations, respectively. The elevation corrections of the Agassiz ice core also increase the discrepancy of  $\delta^{18}\text{O}$  between the Agassiz Ice Cap and NGRIP. This elevation corrections is done using same Dansgaard and ECHAM elevation relation, which leads to an estimated 755 m and 558 m of ice thinning in the middle of Greenland, respectively. The Greenland temperature difference with respect to Ellesmere Island is calculated by assuming non-homogeneous climate over this region. The results indicate a difference of 3 °C between Ellesmere and Greenland without elevation correction of the Agassiz ice core. With elevation correction, temperature difference increases the discrepancy between Agassiz and NGRIP temperature up to 4.9 °C and 6.7 °C using the Dansgaard and ECHAM elevation relations, respectively.

# Contents

<b>1</b>	<b>Introduction</b>	<b>5</b>
<b>2</b>	<b>Scientific Background</b>	<b>9</b>
2.1	Oxygen Isotopes . . . . .	9
2.2	Elevation Reconstruction . . . . .	10
2.2.1	Lapse rate . . . . .	10
2.2.2	ICE-6G_C . . . . .	11
2.3	Glacial Isostatic Adjustment (GIA) . . . . .	13
2.4	Radiocarbon Dating . . . . .	16
2.4.1	Marine Reservoir Effect . . . . .	17
<b>3</b>	<b>Data and Methods</b>	<b>20</b>
3.1	Ice Core Data . . . . .	20
3.1.1	Northern Canada-Agassiz Ice Cap . . . . .	20
3.1.2	Northern Canada-Devon Ice Cap . . . . .	22
3.1.3	Greenland-NGRIP . . . . .	22
3.2	ICESHEET Program . . . . .	25
3.2.1	Shear Stress . . . . .	28
3.2.2	Topography . . . . .	29
3.2.3	GIA . . . . .	30
3.2.4	Sea Level Test . . . . .	31
3.3	Elevation Correction . . . . .	32
3.3.1	ECHAM-wiso . . . . .	33

<b>4</b>	<b>Results and Discussion</b>	<b>37</b>
4.1	Ice Sheet Reconstruction . . . . .	37
4.1.1	Relative Sea Level . . . . .	37
4.1.2	Elevation and Ice Thickness . . . . .	42
4.2	Correction of $\delta^{18}\text{O}$ . . . . .	42
4.2.1	Agassiz Ice Cap . . . . .	42
4.2.2	Devon Ice Cap . . . . .	49
4.3	Greenland . . . . .	49
4.3.1	Homogeneous Climate . . . . .	53
4.3.2	Non-homogeneous Climate . . . . .	57
4.4	Summary . . . . .	58
<b>5</b>	<b>Conclusion and Outlook</b>	<b>60</b>
	References . . . . .	63

# Chapter 1

## Introduction

Changes in the spatial and temporal distribution of insolation received by Earth cause climate change. Different orbital parameters, specifically eccentricity, obliquity, and precession, determine the intensity of insolation [Milankovitch, 1930]. The orbital parameters change very gradually over many thousands of years. Changing solar radiation directly influences the Earth's climate system, thus impacting the advance and retreat of Earth's glaciers. In the late Quaternary period (the past one million years), there was a series of glacial-interglacial cycles that had a period of approximately 100,000 years [Imbrie et al., 1992]. Having more knowledge about climate change during these cycles can lead us to better understand current climate change. It can also be used to evaluate climate models for better prediction of the future. Glacial-interglacial climate changes are documented by climate proxy records [Imbrie et al., 1992; Tzedakis et al., 1997], largely derived from deep sea sediments, tree-rings, and ice cores.

In this thesis, I study the ice sheet history in northern Canada since the Last Glacial Maximum (LGM) until present time. The main question of this project is why two close locations such as Northern Canada and Greenland respond differently to climate change. Although Greenland and Canadian Arctic Archipelago are part of the North American Plate and they are close to each other, modern ice conditions in these two regions are very different. Greenland is the only existing ice sheet in the Northern Hemisphere, but ice on the Canadian Arctic Archipelago is restricted

Table 1.1: The mass and percent natural abundance for oxygen isotopes. The isotopic mass data are from Audi and Wapstra (1993, 1995). The percent natural abundance data are from the 1997 report of the IUPAC Subcommittee for Isotopic Abundance Measurements by Rosman and Taylor (1998).

Isotopes Symbol	Mass of Atom (u)	Abundance (%)
$^{16}\text{O}$	15.994915	99.632
$^{17}\text{O}$	16.999132	0.038
$^{18}\text{O}$	17.999160	0.205

to high altitude ice caps. Geological data from these islands show that in the Last Glacial Maximum, the Innuitian Ice Sheet covered them completely [Blake Jr, 1970; Prest, 1969], and looked very similar to the presently glaciated Greenland [England et al., 2006]. The Innuitian Ice Sheet, at its maximum extent, coalesced with the Greenland Ice Sheet to the east and the Laurentide Ice Sheet to the south. During the early Holocene, the ice sheet retreated. In contrast, the Greenland Ice Sheet remained relatively stable during the Holocene and has not trended towards complete deglaciation.

Ice cores are used to understand past climate, the growth and retreat of large ice sheets, and to measure signals of periodical climate change. Measuring the stable isotopic composition of elements in geological archives helps us to find out information about the past climate. Isotopes of elements have the same number of protons and different number of neutrons. Isotopes have different atomic mass but the same chemical properties. The abundance of specific isotopes is different [Criss, 1999]. Oxygen, for instance, is composed of three stable isotopes,  $^{16}\text{O}$ ,  $^{17}\text{O}$ , and  $^{18}\text{O}$ .  $^{16}\text{O}$  is the most abundant and lightest oxygen stable isotope. Table 1.1 shows the natural abundance in percentage and atomic mass with the unified atomic mass unit, symbol u, defined as  $\frac{1}{12}$  of the atomic mass of one  $^{12}\text{C}$  atom in its electronic and nuclear ground states.

Water isotopes are formed by combination of oxygen and two hydrogen atoms. The majority of water molecules contain  $^{16}\text{O}$ . While water enriched in the heavier oxygen isotopes, which means  $^{17}\text{O}$  or  $^{18}\text{O}$ , called heavy-oxygen water. The isotopic

composition of water varies in different phases. Condensation and precipitation during air-mass cooling preferentially remove heavy water, depleting the air mass of heavy water. So that further precipitation becomes progressively lighter. The colder an air mass is, the more depleted of heavy water it becomes and the lighter the precipitation it produces [Dansgaard, 1964; Robin, 2010]. The relative ratio of  $^{18}\text{O}/^{16}\text{O}$  is measured in "per mil" (‰ parts per thousand). The  $\delta^{18}\text{O}$  value can be used as a proxy for temperature, which will be discussed in chapter 2. Ice cores can be used for such studies, because of their formation over thousands of years. Ice cores give access to local temperature and precipitation rates over long periods of time. They are also unique because the entrapped air provides direct records of past changes in atmospheric trace-gas composition [Bradley, 1999].

In this project, the  $\delta^{18}\text{O}$  data from ice cores of two ice caps (The Agassiz and Devon Ice Caps) will be compared to Greenland's  $\delta^{18}\text{O}$  (NGRIP) during overlapping timescales. The positions of the ice cores are shown in Fig. 1.1. Since there is a strong relationship between  $\delta^{18}\text{O}$  and the elevation of an ice sheet [Epstein, 1959; Dansgaard, 1961], information about surface elevation evolution is needed to correct temperature data to compare records, which will be discussed more in Chapter 2. One of the complicating factors in Canadian Arctic climate records is the high rate of glacial isostatic adjustment (GIA) (Chapter 2), which has been reported to account for upwards of 40% of the climatic signal in these ice core records [Koerner and Fisher, 1990]. Thus, it is important to use an ice sheet reconstruction, which includes GIA to correct  $\delta^{18}\text{O}$ .

To evaluate the elevation and ice thickness in this region, the ICE-6G reconstruction is used as a first step to reveal the significance of elevation changes and the GIA effect. Then, the Innuitian Ice Sheet is reconstructed with the methodology of Gowan et al. (2016a,b) to show the position of ice sheets and their retreat through the time. A large number of parameters can affect ice sheets growth and retreat. This makes past ice sheet reconstruction complex. The advantage of the method I use is that it produces a physically realistic ice sheet reconstruction with minimal

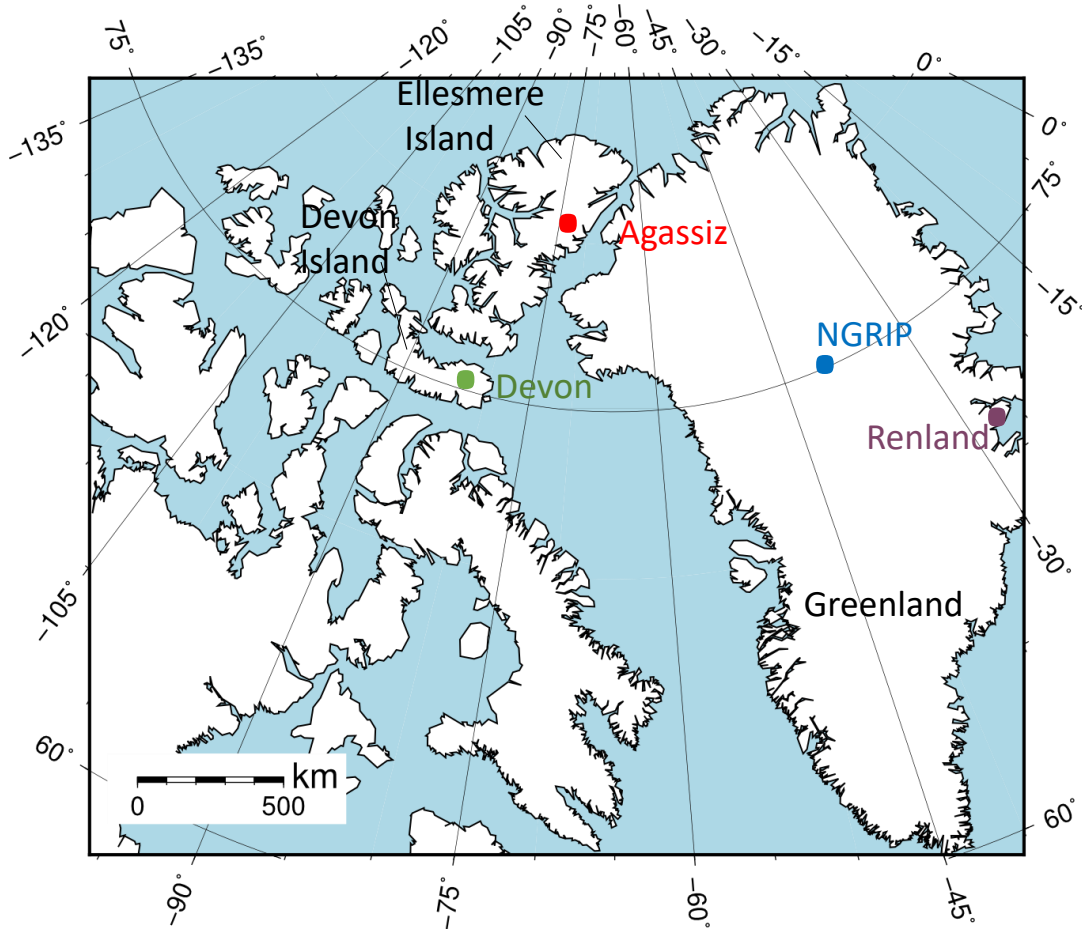


Figure 1.1: The location of different ice cores that are studied in this project. The shoreline configuration is for present time.

assumptions. The reconstruction are based on the assumption of perfectly plastic and steady-state ice condition. There are three non-climatic and dynamic parameters as inputs: ice margin, basal shear stress and basal topography. Description of this methodology and results are shown in Chapters 3 and 4.

corrected  $\delta^{18}\text{O}$  for elevation changes and the difference between  $\delta^{18}\text{O}$  in Greenland and northern Canada are provided in Chapter 4. Also, the variation of elevation in these three sites is shown during the past 20 ka (thousand years before present). The result will be analysed and discussed in this chapter as well.



# Chapter 2

## Scientific Background

### 2.1 Oxygen Isotopes

To analyse past climate, the isotopic composition of water in an ice core must be evaluated. The variation of oxygen isotopic composition in the ice cores reveals information about atmospheric temperature. The heavy isotope content in precipitation decreases with condensation temperature [Dansgaard, 1953, 1954]. To quantify this, the isotopic ratio of the sample relative to a standard sample is needed. It is defined as  $\delta$  in Eq. 2.1.

$$\delta(\text{‰}) = \left( \frac{R_{\text{sample}}}{R_{\text{Standard}}} - 1 \right) \times 1000 \quad (2.1)$$

The  $\delta$  value could be applied to any isotopes in Eq. 2.1, but in this study  $R_{\text{sample}}$  and  $R_{\text{standard}}$  are the ratio of  $^{18}\text{O}/^{16}\text{O}$ . The standard isotopic composition of water is Vienna Standard Mean Ocean Water (VSMOW), which represents the present day isotopic composition of ocean. The International Atomic Energy Agency (IAEA) promulgated this standard as  $R_{\text{standard}} = (2005.20 \pm 0.43) \times 10^{-6}$ .

The relation between temperature and  $\delta^{18}\text{O}$  is highly correlated, so  $\delta^{18}\text{O}$  can be used as a paleothermometer. The  $\delta^{18}\text{O}$  records at different sites will be discussed in Chapter 3.

## 2.2 Elevation Reconstruction

The temperature reconstruction of Greenland and Northern Canadian Archeology is the objective of this thesis. As described in Chapter 1, the  $\delta^{18}\text{O}$  is related to the temperature. Converting  $\delta^{18}\text{O}$  to temperature is possible using obtained linear relationship between  $\delta^{18}\text{O}$  and temperature [Johnsen et al., 1989; Dansgaard and Gundestrup, 1973; Cuffey et al., 1994]. The elevation and temperature are related as well (discussed in Section 2.2.1). Since the O18-temperature relation provides the temperature without considering elevation changes, if the elevations of sites change during the time, the correction of the temperature reconstructions based on elevation changes are needed [Epstein, 1959; Dansgaard, 1961]. In order to apply this correction, the elevation history of the sites has to be studied. To do so, I use ICE-6G reconstruction as a base reconstruction (Section 2.2.2). Subsequently, I reconstruct the Innuitian Ice Sheet (Chapter 3).

### 2.2.1 Lapse rate

The relation between temperature and elevation is called lapse rate, which models the decline of  $\delta^{18}\text{O}$  with increasing elevation. The adiabatic lapse rate is the rate of temperature change with elevations change, when the air parcel adiabatically (without transfer heat or matter) goes up [Kittel and Kroemer, 1980]. The simplest equation for dry adiabatic lapse rate is Eq. 2.2, where  $g$ ,  $c_p$ ,  $\Gamma_d$ ,  $T$ , and  $z$  represent Earth's gravitational acceleration, the specific heat of dry air at constant pressure, adiabatic lapse rate, temperature, and altitude respectively.

$$\Gamma_d = -\frac{dT}{dz} = \frac{g}{c_p} \quad (2.2)$$

An early derivation of the lapse rate was  $6.5 \text{ K km}^{-1}$  [Brunt, 1933]. Stone and Carlson (1979) estimated that the hemispheric annual mean adiabatic lapse rate was  $5.67 \text{ K km}^{-1}$ .

### 2.2.2 ICE-6G\_C

There are different reconstructions for ice sheets, with diverse assumptions and different configurations (i.e [Peltier et al., 2015](#); [Lambeck et al., 2017](#); [Gowan et al., 2016b](#); [Lecavalier et al., 2017](#)). To get an initial estimation of elevation change in this region, I use the global ICE-6G\_C (VM5a) model as a base reconstruction in northern Canada and Greenland after Last Glacial Maximum (LGM), when the ice sheets were at their greatest extent [[Peltier et al., 2015](#)].

ICE-6G\_C is a reconstruction of the ice thickness and surface elevation for the major ice sheets through the LGM to the present [[Peltier et al., 2015](#); [Argus et al., 2014](#)]. The model of Earth rheological structure they used was labelled VM5a for calculating GIA. The model resolution is a  $1^\circ \times 1^\circ$  degree global grid, and presents different variables such as, land area fraction, ice area fraction, topography difference from present, topography, orography, and thickness of the ice sheet. In this reconstruction, GIA has been used for reconstructing the ice sheets, which will be discussed in section 2.3.

The variation of ice thickness from 25 ka to present at 5000 year time intervals is shown in Fig. 2.1. The major difference is between 15 ka (Fig. 2.1d) and 5 ka (Fig. 2.1b). Other intervals do not significantly vary. There is no significant change after 20 ka in the ice sheets, they remained in their maximum extent until 25 ka.

The ice margin data that are used in this project, is based on reconstructions by [Dyke \(2004\)](#). These reconstruction are in radiocarbon age with 500 years intervals. They were converted to calendar years by assuming error of 250 years, and calibrating them with the OxCal program [[Ramsey, 1995](#)]. Calibration is needed, mainly because the proportion of  $^{14}\text{C}$  in the atmosphere is not constant within time. It is important because the radiocarbon age is calculated relative to this proportion, which is discussed in section 2.4. Since the calendar age is not exactly the same as the ICE-6G ages, the closest date was chosen. These are shown in Table 2.1 [[Gowan, 2013](#)].

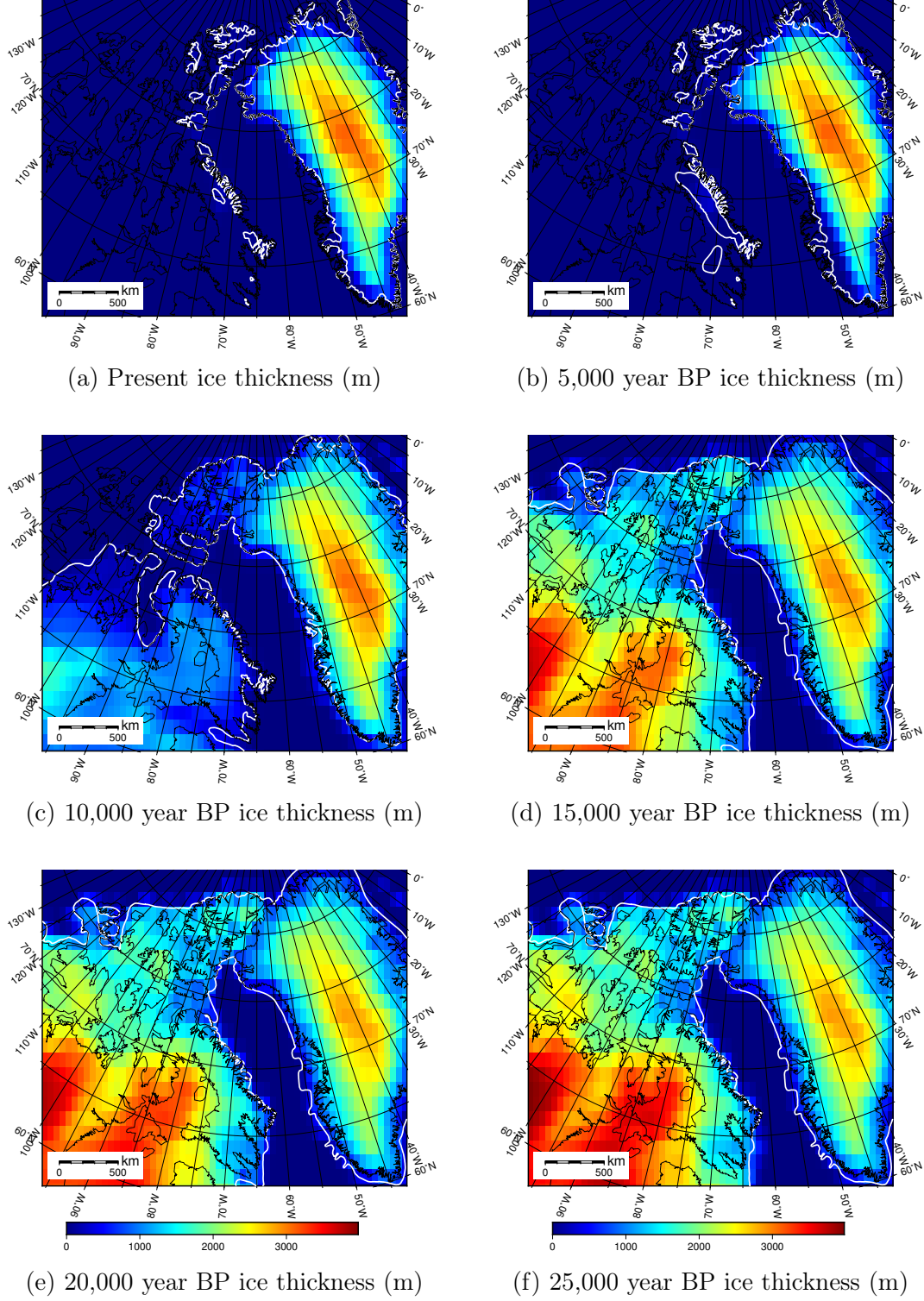


Figure 2.1: Ice thickness in the Greenland and Innuitian Ice Sheet from LGM to Present using the ICE-6G reconstruction [Peltier et al., 2015; Argus et al., 2014] in meters. The white lines determine ice margin based on Dyke (2004), the corresponding age is presented in Table 2.1.

Table 2.1: Conversion of radiocarbon ages to calendar years and corresponding years of the ICE-6G [Gowan, 2013]. The first and third columns are in calendar year (cal yr), the second one is in radiocarbon year.

Calendar (cal yr BP)	Radiocarbon ( $^{14}\text{C}$ yr BP)	ICE - 6G (cal yr BP)
5800	5000	5000
10100	9000	10000
11600	10000	11000
12000	10250	12000
12900	11000	13000
13900	12000	14000
15700	13000	15000
20200	17000	20000
21500	18000	25000

## 2.3 Glacial Isostatic Adjustment (GIA)

The interior of the Earth has different layers: an outer silicate solid crust, a viscous mantle, a liquid outer core, and a solid inner core (Fig. 2.2). When a sufficient surface load, such as ice sheet during the glacial times, is applied to the crust, it will deform elastically [Peltier and Andrews, 1976]. In addition, the viscoelastic mantle has a viscous deformation component in addition to an elastic component. The mantle flows away from the loaded region. At the end of each glacial period after the ice sheets retreat, the elastic component uplifts immediately, while due to the extremely high viscosity of the mantle, the viscous component will take thousands of years to reach an equilibrium level. This gradual uplift is the residual GIA. Modern GIA theory was originally developed in a series of papers published in the 1970s [Peltier, 1974, 1976; Farrell and Clark, 1976; Peltier and Andrews, 1976; Clark et al., 1978; Peltier et al., 1978]. As the North America continent was covered by the Laurentide and Innuitian Ice Sheet during the last glaciation, retreat of them after LGM resulted in vertical motion of the Earth's surface. Vertical velocities around Hudson Bay, for instance, show a present-day uplift of about 10 mm/yr [Sella et al., 2007]. Hudson Bay is located near the centre of the Laurentide Ice Sheet at the LGM.

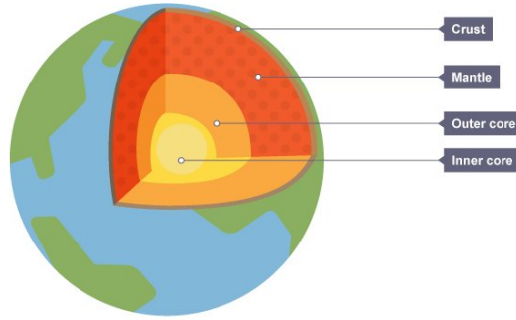


Figure 2.2: Structure of the Earth [Simpetru].

Where GIA is significant, changes in ice thickness alone cannot explain all elevation changes. It is important to obtain surface elevation change including GIA and use it for correcting  $\delta^{18}\text{O}$  data. Comparison between Fig. 2.3, which shows surface elevation, and Fig. 2.1, which shows ice thickness, demonstrates the influence of changing topography. The ice thickness, for instance, increased in central of Greenland between 25 ka to 5 ka, while surface elevation did not change significantly due to land depression.

GIA plays a role in determining the discrepancy between ice thickness and elevation changes. The variation of elevation in the three ice cap locations is presented in Fig. 2.4. The variation at NGRIP is different from the Canadian ice cores. The surface elevation increases (about 230 m) with small oscillation until reaching maximum elevation around 8 ka (3.4 km). Then, it slightly decreases to reach stability for 3000 years. It has been stable for thousands of years since then at 2.96 km (Fig. 2.4a).

The Agassiz and Devon ice core locations have experienced different elevation variations than at NGRIP. The largest elevation change occurred in the Agassiz ice cap (about 950 m). The Agassiz Ice Cap was stable until 13 ka at 2.2 km elevation, then decreased to approximately 1.2 km, at 8 ka. The surface elevation has been more or less stable after that time, with a slight upward tendency, as a result of GIA (Fig. 2.4b). The Devon Ice Cap follows this pattern as well, although, its decline is significantly less than Agassiz (about 190 m). Another difference is that the retreat happened earlier (around 15 ka BP). When the Devon Ice Cap reached its



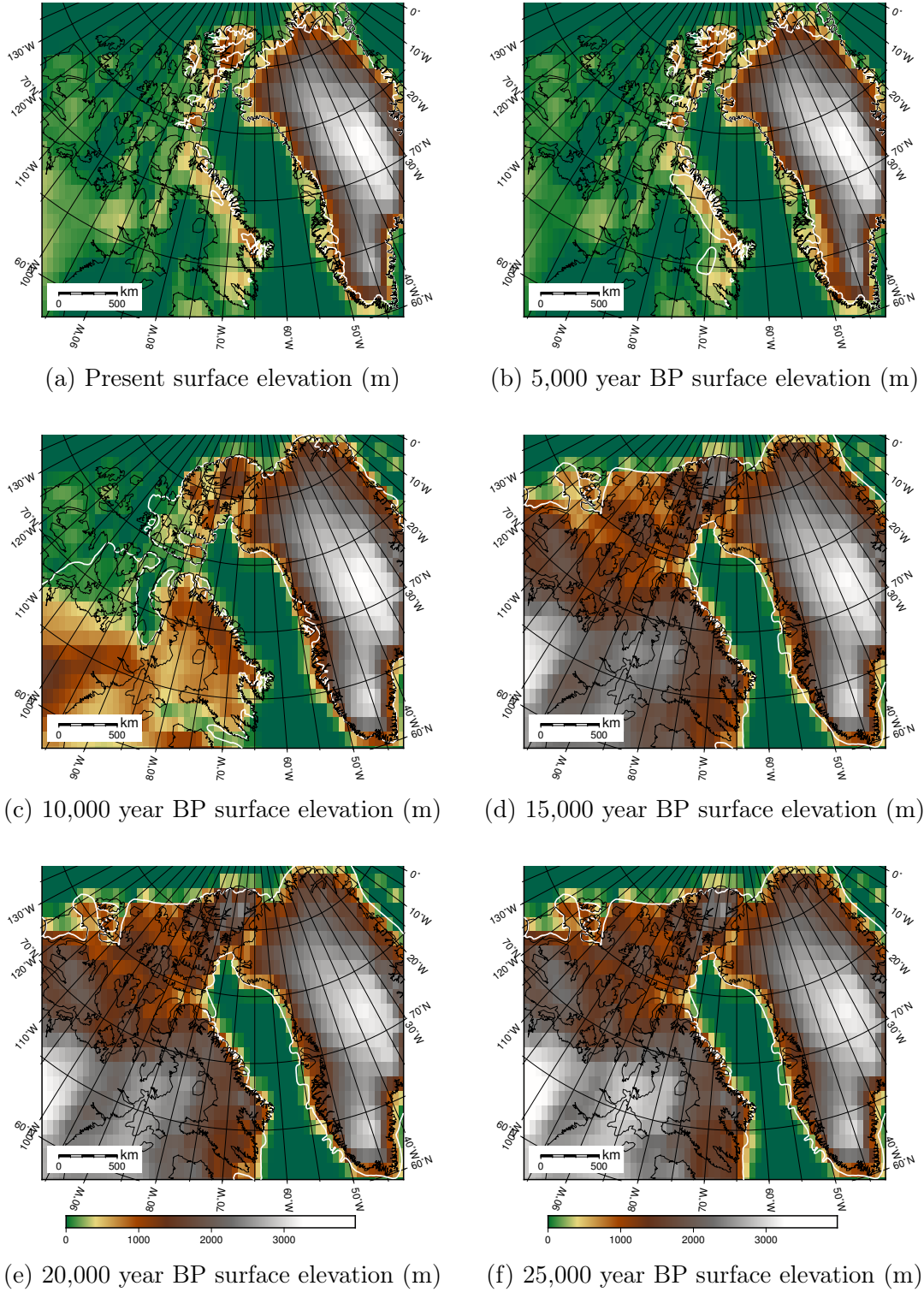


Figure 2.3: Surface elevation in the Greenland and Innuitian Ice Sheet from LGM to present using the ICE-6G reconstruction [Peltier et al., 2015; Argus et al., 2014] in meters. The white lines determine ice margin based on Dyke (2004), the corresponding age is presented in Table 2.1.

first minimum elevation, Agassiz had just started retreating. The current elevation for the Devon Ice Cap is 1.3 km (Fig. 2.4c).

One method for estimating volume and elevation of ice sheet in glacial time is based on magnitude of GIA in that area, which is used in the ICE-6G model [Peltier et al., 2015]. Relative sea level data is used for evaluating GIA. When the land is depressed by a large ice sheet, relative sea level can be hundreds of meter higher than present immediately after the ice retreated [Farrell and Clark, 1976]. Radiocarbon dates on material that indicates sea level relative to the samples' present elevation is used in the chronology of relative sea level data, which is discussed in the following section.

## 2.4 Radiocarbon Dating

The radioactive isotope of carbon,  $^{14}\text{C}$ , can be used to determine the age of organic material. Organic material refers to the remains of carbon based organisms. The radiocarbon dating method is based on the fact that  $^{14}\text{C}$  is produced naturally in the atmosphere by interaction of nitrogen and cosmic rays that bombard the Earth [Wallace and Hobbs, 2006]. Radiocarbon  $\text{CO}_2$ , which is produced by oxidizing  $^{14}\text{C}$ , gets into the food chain through the photosynthesis of plants. As long as the organism is alive, it exchanges carbon with its environment. The ratio of  $^{14}\text{C}$  in the atmosphere and organisms should be the same for plants. The cycle is stopped by death of the organism, and  $^{14}\text{C}$  it contains declines because of radiocarbon decay, and the ratio of  $^{14}\text{C}$  to  $^{12}\text{C}$  will gradually decrease [Valkovic, 2000]. Measuring the remaining amount of  $^{14}\text{C}$  gives information about its time of death. This information can be used, for instance, to figure out the past sea level elevation dating elevated marine or terrestrial material are used. However, the reliability of some materials is debatable. An animals' nutritional habits can change the uncertainty. For example, if the creature eats mud, it is probable that it eats material which can be thousand years died [England et al., 2013]. Consequently, dating by the amount of  $^{14}\text{C}$  is not reliable for these fossils (overestimated age).

The internationally accepted half-life of  $^{14}\text{C}$ , since the early 1960s, is 5730 years,



which is obtained by revising of initial Libby half-life. The half-life used for calculating the radiocarbon age of most geologic and paleontological samples is the Libby half-life, 5568 years [Libby, 1952], to keep consistency with early papers and avoid double correction.

After obtaining the age in radiocarbon year, it is necessary to convert it to calendar age. This two ages are different because the production rate of radiocarbon in the atmosphere has varied by a few percent over time. This variation is known due to change in the cosmic ray flux, geomagnetic field intensity, and carbon cycle [Mazaud et al., 1991; Laj et al., 1996; Voelker et al., 2000; Beck et al., 2001]. To convert to calendar dates a calibration curve is needed, which is created by radiocarbon dating of something that has a known age, such as tree rings. This is done using the OxCal 4.2 program [Ramsey, 2009].

### 2.4.1 Marine Reservoir Effect

The basic assumption of radiocarbon dating is that concentrations of  $^{14}\text{C}$  in the atmosphere and therefore in all living organisms are in equilibrium. However, the  $^{14}\text{C}$  concentration in ocean is different from atmosphere. The surface layer of the ocean gets carbon dioxide from atmosphere, but the deep ocean contains different ratio of  $^{14}\text{C}$  because of radioactive decay that has already occurred in water at the bottom of oceans. Consequently, oceans have less  $^{14}\text{C}$  as compared with the atmosphere, which means samples from marine organisms like shells, whales, and seals appear older [Bowman and Leese, 1995]. To cope with this discrepancy, it is necessary to apply a marine reservoir correction to the samples. One way to estimate the correction is to use a program like OxCal [Ramsey, 1995], which is using the 2009 marine calibration dataset [Stuiver and Reimer, 1993; Ramsey, 1995]. There are two curves, marine and atmospheric curves, to calculate the calendar age. This is done by using the IntCal13 and Marine13 calibration curve [Reimer et al., 2013].

For reservoir corrections we use simulated values presented by Butzin et al. (2017) instead of using Stuiver and Reimer (1993) marine reservoir. Butzin et al. (2017)

simulated the spatial and temporal variability in marine radiocarbon ages of surface waters using a three-dimensional ocean circulation model covering the past 50,000 years. So, instead of reservoir correction of tropical regions like [Stuiver and Reimer \(1993\)](#), it is accurate to use the spatial and temporal marine radiocarbon ages.

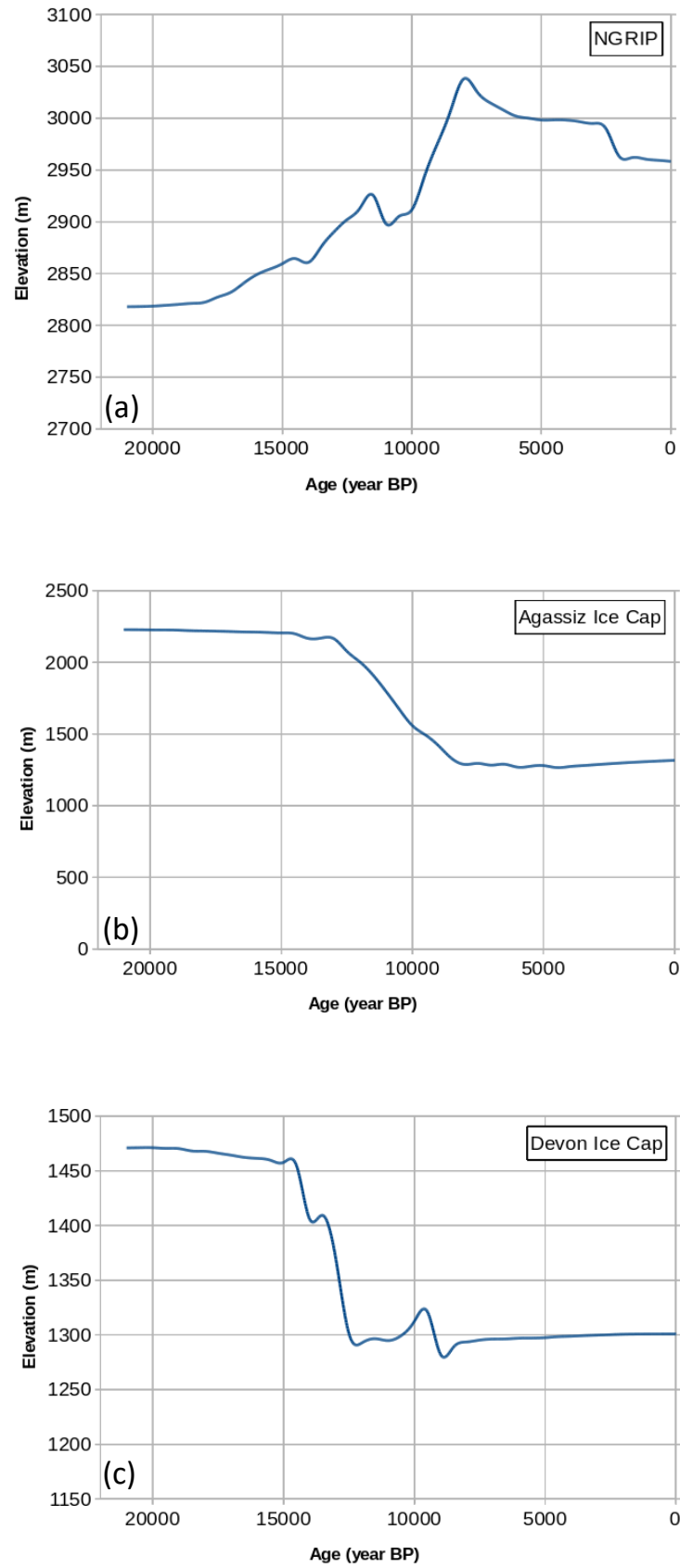


Figure 2.4: Surface elevation of a) NGRIP (75.10 °N, 42.32 °W), b) the Agassiz (80.7 °N, 73.1 °W), and c) the Devon ice cap (75.34 °N, 82.17 °W) based on the ICE-6G reconstruction [Peltier et al., 2015; Argus et al., 2014].

# Chapter 3

## Data and Methods

### 3.1 Ice Core Data

Regional temperature differences could explain the different history of two ice sheets.  $\delta^{18}\text{O}$  from ice cores, as described in Chapter 2, represents the temperature at the core location through time. From the Innuitian Ice Sheet, there are time series of  $\delta^{18}\text{O}$  data for the Devon and Agassiz Ice Caps during the Holocene. From Greenland Ice Sheet, more ice cores have been extracted, but I choose NGRIP from central part of Greenland, which is not close to margins and is not affected by changes in ice margin.

#### 3.1.1 Northern Canada-Agassiz Ice Cap

The Agassiz Ice Cap is on the central eastern side of Ellesmere Island in Canada (Fig. 1.1). The drilling site is located at 80.7 °N, 73.1 °W at an elevation of 1700 m. Four ice cores were collected, A77, A79, A84, and A87. The A84 and A87 cores were drilled within a 30 m distance of the dome. The dome of the ice sheet is usually located at the highest elevation location and ice flows away from this point. The A79 ice core was drilled 1300 m southwest of the dome. The A77 ice core was drilled around 2300 m south of the dome [Fisher et al., 1995].

The Agassiz ice cores have been matched to the NGRIP ice core using volcanic reference horizons, detectable by Electrical Conductivity Measurements (ECM) [Vinther

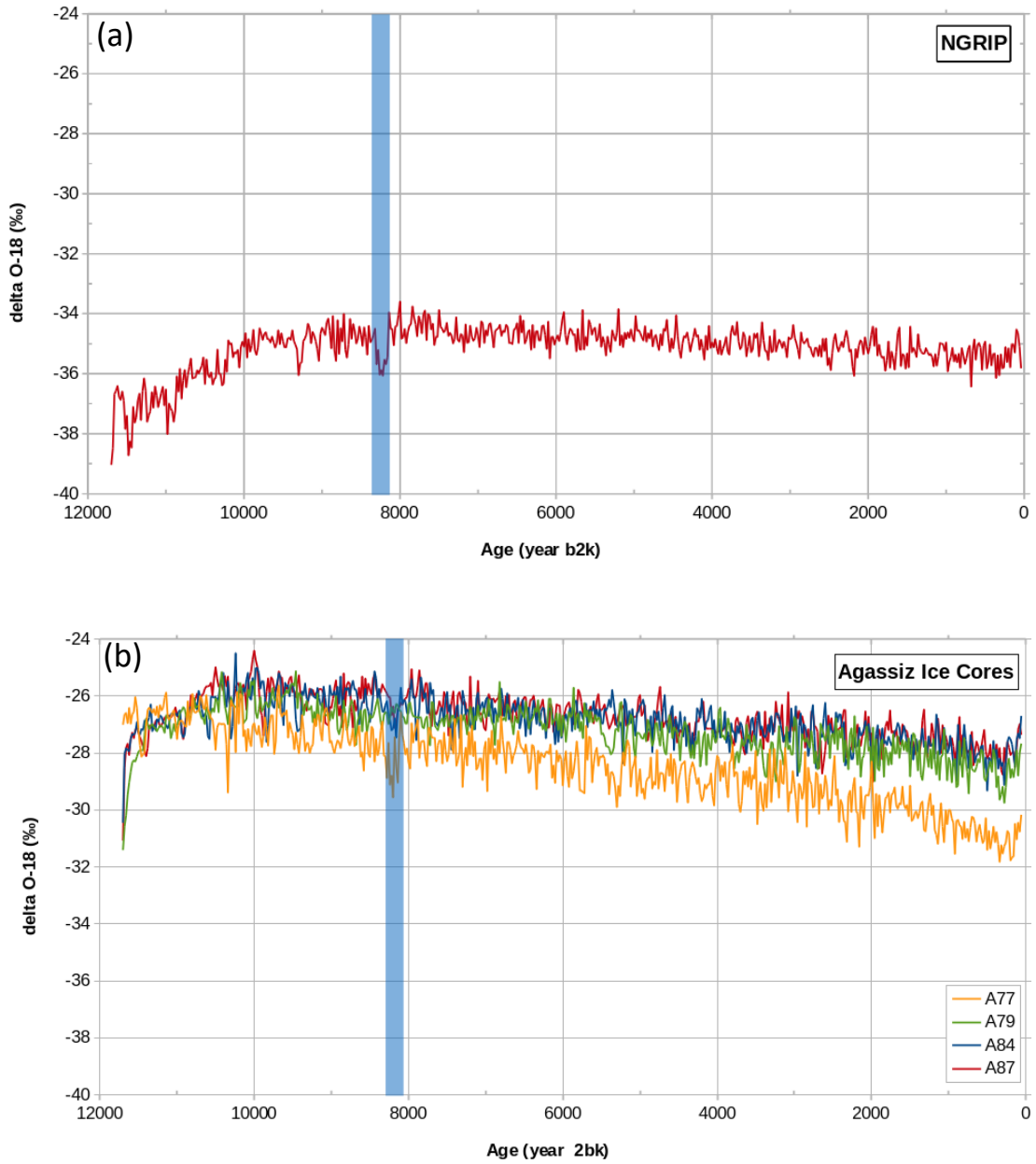


Figure 3.1:  $\delta^{18}\text{O}$  data on GICC05 timescale in a) North Greenland Ice Core, b) Agassiz ice core; blue column illustrate 8.2 ka event. [Fisher et al., 1995; Vinther et al., 2006; Rasmussen et al., 2006].

et al., 2008] with the GICC05 timescale (the uncertainties can be found in Vinther et al. (2006)). The ECM is based on difference between electrical conductivity of ice and ashes. ECM have been carried out on the A77, A79, and A84 ice cores by Zheng et al. (1998). The fluctuation of  $\delta^{18}\text{O}$  since 12000 ka is shown in Fig. 3.2b with 20 years resolution.

### 3.1.2 Northern Canada-Devon Ice Cap

The Devon Ice Cap is on eastern Devon Island, located at 75.34 °N and 82.17 °W (Fig. 1.1). Three ice cores were collected in 1971, 1972, and 1973 from this site. The data discussed in this project are the cores drilled in 1973 and 1972 [Fisher, 1976; Fisher and Koerner, 1981; Fisher, 1979; Fisher et al., 1983]. The ice cores reached bedrock at depths of 298.9 m and 299.4 m [Paterson et al., 1977]. The time scale for the cores has been discussed at length by Paterson et al. (1977) and Koerner and Fisher (1981). The timescale was checked by absolute dating of ice at four points by  $^{32}\text{Si}$  [Clausen, 1973] and at another four points by  $^{14}\text{C}$  based on  $\text{CO}_2$  extracted from air bubbles in the ice [Oeschger et al., 1976]. After that, the cores have been cross-correlated with those from Camp Century in Greenland [Hammer et al., 1978].

For a comparison of  $\delta^{18}\text{O}$  between the Devon and NGRIP records, the starting points and time intervals should be the same. Similar resolution has been chosen (50 years), but the starting points are different. The Devon ice core data set has a starting point at AD 1961, while in NGRIP it is AD 2000. Linear interpolation was used to align the data. The changes of  $\delta^{18}\text{O}$  during the past 19 ka in both sites are presented in Fig. 3.2.

### 3.1.3 Greenland-NGRIP

In Greenland, several ice cores have been drilled since the mid of 1960s [e.g. Hansen and Langway Jr, 1966; Vinther et al., 2009]. In this project, the Northern Greenland Ice Core Project (NGRIP) was chosen to represent Greenland for comparison with the northern Canada ice cores. It is located at 75.10 °N and 42.32 °W at an elevation of 2917 m and an ice thickness of 3085 m. There are data sets with different timescales and resolutions at this site. Two different data sets with 20 year resolution and 50 year resolution were chosen, to have the same resolution as the Agassiz and Devon Ice Caps, which have the resolution of 20 year and 50 year, respectively. The data are from Vinther et al. (2006), Rasmussen et al. (2006), and Andersen et al. (2004). All data are downloaded from the contribution of World

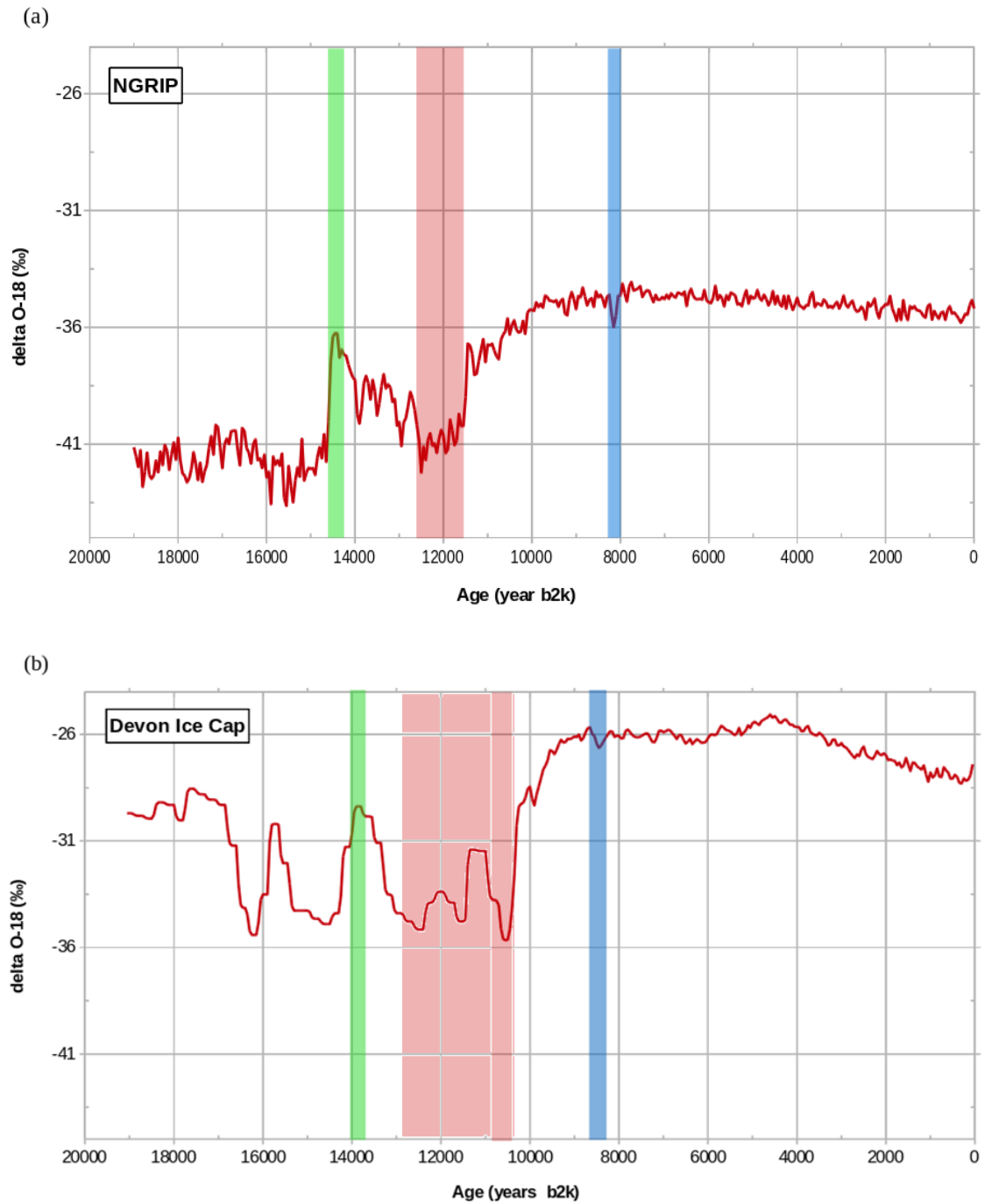


Figure 3.2:  $\delta^{18}\text{O}$  data in a) North Greenland Ice and, b) Devon ice core; blue, red, and green illustrate climate event, 8.2 ka, Younger Dryas, and the Boelling-Alleroed interstadial respectively. [Fisher, 1976; Andersen et al., 2004].

Data Center for Paleoclimatology, Boulder, and NOAA Paleoclimatology Program [National Oceanic and Atmospheric Administration].

In the 20-year-resolution data set, the data from 0 ka to 7.9 ka are described in [Vinther et al. \(2006\)](#) and the data from 7.9 ka to 14.7 ka are in [Rasmussen et al. \(2006\)](#). Also, the Greenland Ice Core Chronology 2005 (GICC05) timescale is used, which is based on many overlapping data series from the three different cores (NGRIP, GRIP, and DYE-3). Overlaps between different sections ensure consistency between the different parts of the timescale. They used electrical conductivity measurements (ECM) to detect volcanic reference horizons on the cores, which exist in the entire NGRIP core [[Dahl-Jensen et al., 2002](#)]. The  $\delta^{18}\text{O}$  data until 12 ka is shown in Fig. 3.1a.

A 50-year-resolution data set [[Andersen et al., 2004](#)], for the GRIP's data, with 2001/ss09sea timescale [[Johnsen et al., 2001](#)], was chosen for comparison with Devon. That data are presented in Fig. 3.2a.

The Devon ice core data are similar to NGRIP at the first 10000 years BP (Fig. 3.2), but going back in time the correlation between their  $\delta^{18}\text{O}$  values diminishes. For the Devon ice core,  $\delta^{18}\text{O}$  is increasing between 16 ka to 19 ka, which is not seen in NGRIP at all. The difference between the Devon and NGRIP varies from 7‰ to 10‰ until 10 ka, while between 10 ka and 19 ka, it shows significant fluctuations from 0‰ to 14‰.

Some climate events are color-coded in Fig. 3.1 and Fig. 3.2. Blue columns, represent the 8.2 ka cooling event [[Johnsen et al., 1992a](#); [Dansgaard et al., 1993](#); [Alley et al., 1997](#)]. This is the largest decrease, occurring between 8.4 and 8.0 ka after the end of the Preboreal warming (between 11.5 and 9.5 ka). In the Greenland ice core records, where it was first clearly noted, the 8.2 ka event is the largest abrupt climatic cooling of the Holocene period. It is estimated as a rapid cooling of  $6 \pm 2^\circ\text{C}$  by [Cuffey et al. \(1995, 1994\)](#). The climate during this 8.2 ka event should be cold, dry, dusty, and have low methane concentrations. The reason behind this event is a weakening of thermohaline circulation. This is a consequence of a freshwater pulse, associated with final stages of North American deglaciation [[Renssen et al.,](#)



2001]. The Agassiz ice core and NGRIP data have been synchronized. Thus, the timing and intensity of this event in both ice cores are compatible (Fig. 3.1). However, the Devon ice core does not show the 8.2 ka event as clear as North GRIP and Agassiz. The first decrease after 8 ka is considered to be the 8.2 ka event (Fig. 3.2b).

Since the Devon ice core provides data for a longer period of time, it has more climate events than the Agassiz Ice Cap. In Fig. 3.2a, there is a significant warming around 14.5 ka BP (green column) known as the Boelling and Allerød interstadial (BA) [Kerney et al., 1963; Godwin and Willis, 1961]. This is followed by a series of abrupt returns to glacial climate, the best-known of which is the Younger Dryas event (YD) (red column) [Bard and Broecker, 1992; Stuiver and Reimer, 1993]. The BA is an event between Older Dryas (happened between 15 ka to 14.7 ka Hughen et al. (1996)) and Younger Dryas. The major difference between the Devon ice core and NGRIP  $\delta^{18}\text{O}$  is during the Older Dryas, where  $\delta^{18}\text{O}$  is significantly higher. Its characteristics are similar to the 8.2 ka cooling event. However, the difference between the YD and the 8.2 ka event is that the YD has colder, dryer, dustier, and with lower methane concentration [Johnsen et al., 1992a; Alley et al., 1993; Mayewski et al., 1993; Barnola et al., 1993]. As mentioned before, the Devon Ice Cap does not show any cooling events older than about 10 ka. It may be due to uncertainties of the data in deeper parts of the ice cores.

## 3.2 ICESHEET Program

To take into account the elevation changes of the site in  $\delta^{18}\text{O}$ , we need to reconstruct the ice sheets in these regions. ICE-6G is a global reconstruction and not specially designed for this region. So, it might be not suitable for our purpose. I reconstruct the Innuitian Ice Sheet with the ICESHEET program written by Gowan et al. (2016a). The method was originally established by Reeh (1982) and Fisher et al. (1985).

## Theory

The reconstruction is based on an assumption of steady-state and perfectly plastic ice flow behaviour. Although this assumption is not likely, it does not need to use complicated and unconstrained climatic and ice dynamic parameters. Ice margin, basal shear stress, and topography are three inputs of the program. The basal shear stress ( $\tau_b$ ) is a function of the surface slope ( $\alpha$ ), the thickness ( $H$ ), gravity ( $g$ ) and density ( $\rho$ ) [Nye, 1952]:

$$\tau_b = \rho g H \sin(\alpha) = \rho g H \frac{dE}{ds} \quad (3.1)$$

$E$  is ice elevation and  $s$  is the distance along ice flow line profile. The flow line is the path the glacial flows. In a glacier, because the slope is usually small, so  $\sin(\alpha) = \tan(\alpha) = \frac{dE}{ds}$  could be used. Because I want to reconstruct the ice elevation, the Eq. 3.1 is rewritten as follow.

$$\frac{dE}{ds} = \frac{\tau_b}{\rho g H} \quad (3.2)$$

Reeh (1982) and Fisher et al. (1985) presented expanded version of Eq. 3.2, to solve problems with spatial changes in basal topography and shear stress.

$$\left(\frac{dE}{ds}\right)^2 = \left(\frac{\partial E}{\partial x}\right)^2 + \left(\frac{\partial E}{\partial y}\right)^2 \quad (3.3)$$

In this equation  $x$  points towards the centre of the ice sheet, and  $y$  is parallel to the margin in this coordinate system. Ice elevation is the sum of basal topography ( $B$ ) and ice thickness.

$$E = H + B \rightarrow H = E - B \quad (3.4)$$

Eq. 3.3 and 3.4 is substituted into Eq. 3.2.

$$\left(\frac{\tau_b}{\rho g (E - B)}\right)^2 = \left(\frac{\partial E}{\partial x}\right)^2 + \left(\frac{\partial E}{\partial y}\right)^2 \quad (3.5)$$

The  $x$  and  $y$  coordinates is defined based on the ice margin geometry, and the

Table 3.1: Conversion of radiocarbon ages to calendar years and corresponding years of the ICESHEET [Gowan, 2013]. The first and third columns are in calendar year (cal yr), the second one is in radiocarbon year.

Calendar (cal yr BP)	Radiocarbon ( $^{14}\text{C}$ yr BP)	ICESHEET (cal yr BP)
5800	5000	5000
6300	5500	6000
6900	6000	7000
8000	7200	8000
8900	8000	9000
10100	9000	10000
10900	9600	11000
12000	10250	12000
12900	11000	13000
13900	12000	14000
14700	12500	15000
15700	13000	16000
17100	14000	17000
18200	15000	18000
19200	16000	19000
20200	17000	20000
20800	17500	21000
21500	18000	22000

basal topography ( $B$ ) and shear stress ( $\tau_b$ ) are given as an input variables. Thus, the elevation is obtained from this partial differential equation by the method of characteristics [Reeh, 1982]. The ice sheet model was computed using a minimum resolution of 5 km.

### Ice margin

The reconstruction of the Innuitian Ice Sheet is the objective of this project. However, It is needed to include two bigger ice sheets in the vicinity of the Innuitian Ice Sheet (i.e the Greenland and Laurentide Ice Sheets), because ice sheets change the Earth's surface in their vicinity due to mantle movement. The margins of these three ice sheets are given with a 1000 year interval from 0 to 30000 years BP. For Greenland, the margins of Dyke (2004) are available until 18  $^{14}\text{C}$  yr BP (22000 years BP), which is used in my reconstruction. Corresponding calendar years are given in Table 3.1 [Gowan, 2013]. The ice margin at 30 ka is similar to modern

margin [England et al., 2006], the advance of the Greenland Ice Sheet is estimated with a 1000 year interval between 22 ka and 30 ka. For the Laurentide Ice sheet, the margin of Gowan (2014) with 1000 year intervals is used. Between 20 ka and 30 ka the interval is 2000 years, I interpolated between the margins to reach an interval of 1000 years.

The maximum extend of the Innuitian Ice Sheet was reached around 22 ka [England et al., 2006]. The data from England et al. (2000), England (1999), and England et al. (2004) between 20 ka and 30 ka are used, and calibrated with the OxCal program. The marine reservoir correction is based on model results presented by Butzin et al. (2017). The tools that used for calibrating radiocarbon data were developed by Gowan et al. (2016b). These calibrated data and the flow path of ice sheet (based on geological evidence [England et al., 2006]) are used for determining the ice margin between its maximum extend and 30 ka. The data for northern Canada during this time are limited, consequently, the final ice margin has large uncertainties. After calibration, the data are rounded to four time steps, which are 23 ka, 24 ka, 27 ka, and 28 ka. The location of calibrated data and corresponding margin are presented in Fig. 3.3.

### 3.2.1 Shear Stress

The study area is divided to sub-regions based on bedrock geological age and composition (Fig. 3.4). The initial values were estimated by Gowan (2014) and Gowan et al. (2016b), in the range of  $0.5 \times 10^5$  Pa to  $1.5 \times 10^5$  Pa, on the basis of GIA observations.

Shear stress is not constant through time. In the ICESHEET program there is a maximum shear stress for LGM time and minimum shear stress for near complete retreat for each sub-region. The shear stress is linearly reduced as deglaciation proceeds. The time for starting this linear reduction is assigned to be 2000-4000 years before complete deglaciation. The ice sheet reconstruction is refined by changing the maximum amount of shear stress and starting points of reduction are determined

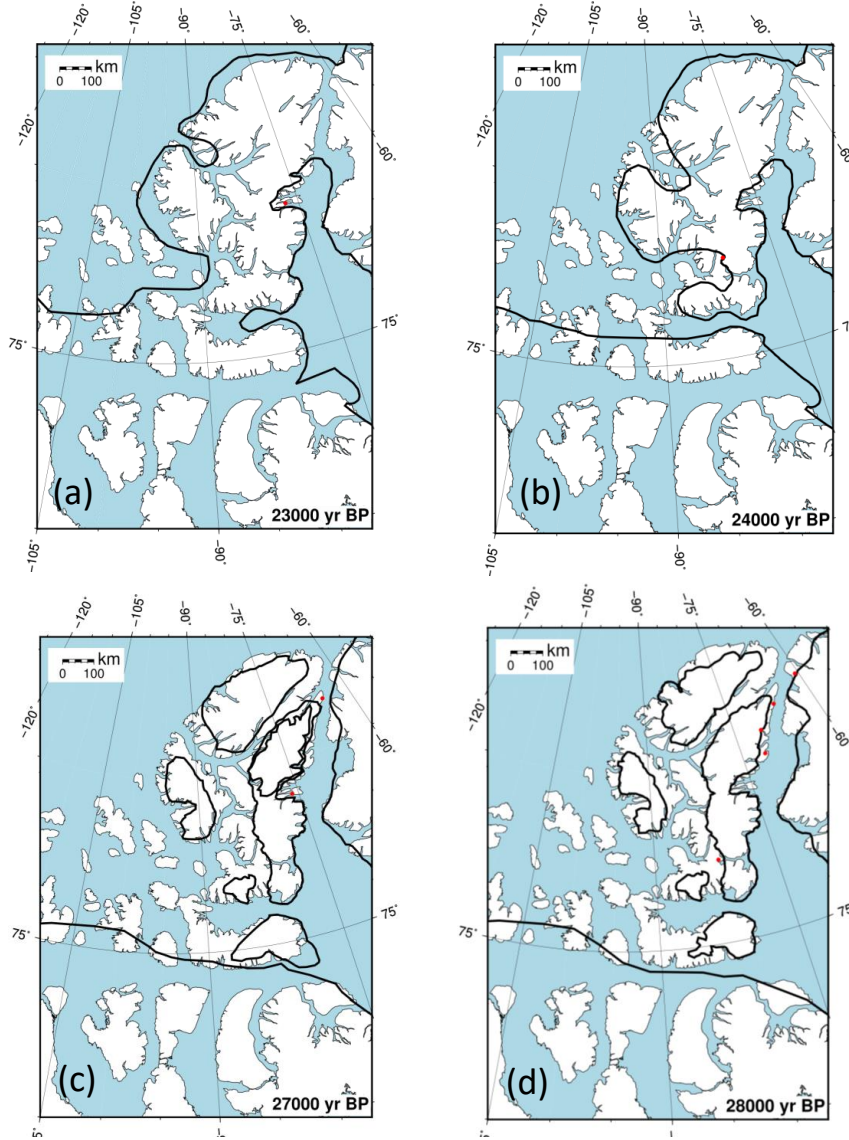


Figure 3.3: Margin reconstruction of a)23 ka, b)24 ka, c)27 ka, and d)28 ka with corresponding data from [England et al. \(2000\)](#); [England \(1999\)](#); [England et al. \(2004\)](#).

due to relative sea level constrains.

### 3.2.2 Topography

According to Eq. 3.5 topography is required for elevation computation. Modern topography is used as a base. After ice volume is estimated for the first time, the calculated deformation of the Earth and sea level change are added to the modern topography. The Rtopo2 data set is used for modern topography in our project [[Schaffer et al., 2016](#)].

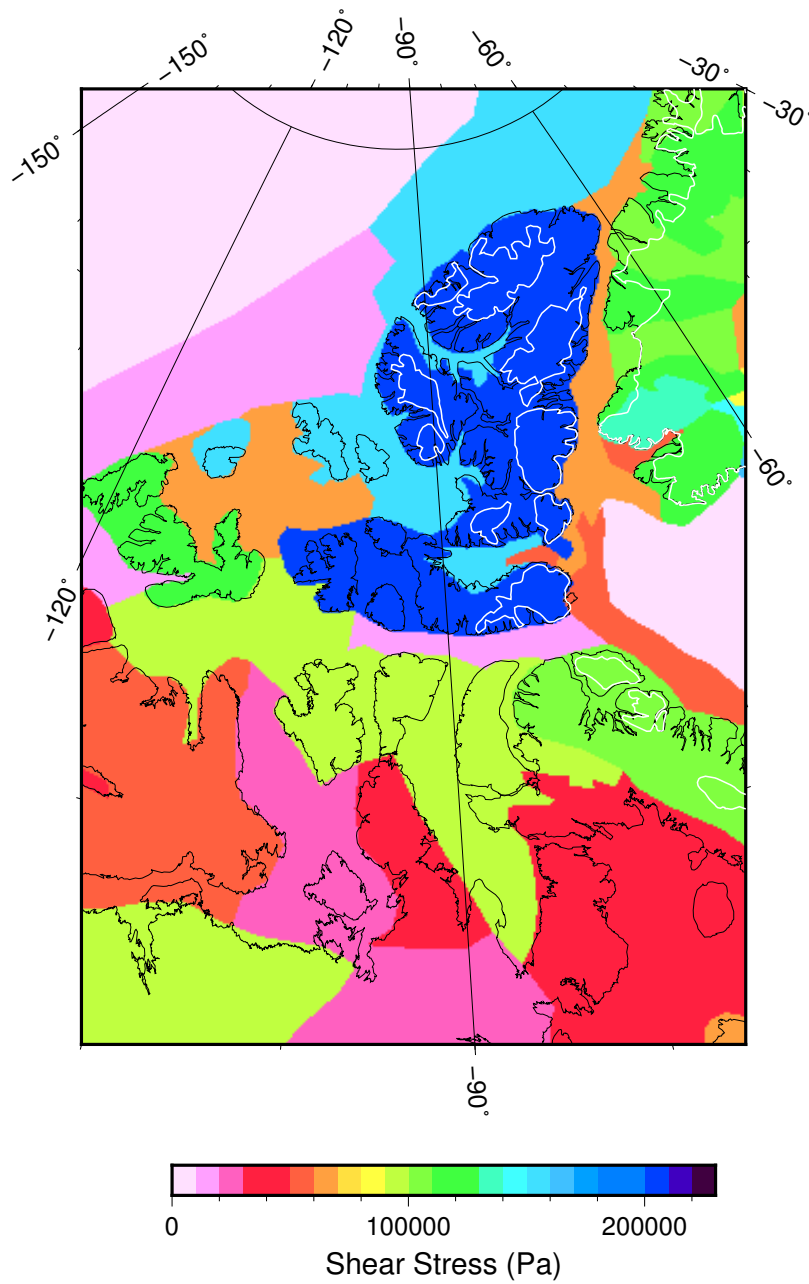


Figure 3.4: Basal shear stress domains and maximum values used for reconstruction. the black lines are the modern day coastlines, the white lines are the current ice margin.

### 3.2.3 GIA

Deformation of the Earth due to surface loading depends on the Earth's structure such as mantle viscosity and lithosphere thickness. Glacial isostatic adjustment is calculated using a spherically radially layered Earth, with an elastic lithosphere and Maxwell visco-elastic mantle and elastic lithosphere. The elastic parameters

are based on the Preliminary Reference Earth Model (PREM) [Dziewonski and Anderson, 1981]. The lithosphere thickness, upper and lower mantle viscosity are 120 km,  $4 \times 10^{20}$  Pa s,  $10^{22}$  Pa s, respectively, based on the preferences of Gowan et al. (2016b). The significant contrast between upper and lower mantle viscosity results from different studies on dynamic topography and geoid data [Forte and Mitrovica, 2001] and mantle flow [Steinberger and Calderwood, 2006; Panasyuk and Hager, 2000]. These values for the lithosphere thickness, upper and lower mantle viscosity are confirmed by Nakada et al. (2017).

### 3.2.4 Sea Level Test

Sea level is define as a vertical hight difference between the equipotential ocean surface and the Earth's solid surface [Milne et al., 2002]. The equipotential ocean surface is the surface of the ocean that would take under the influence of the Earth's gravity and rotation alone. The geiod has constant gravity. The sea level depends on distribution of gravity and the icewater mass exchange on the Earth. Relative sea level (RSL) is the elevation of the past sea level relative to present sea level. Changes in RSL result from changes in absolute sea level and/or movement of Earth's surface and changes in gravity. RSL data are used as benchmarks to assess if the ice sheet reconstruction is realistic. The chronology of RSL indicators can show whether the relative sea level was above or below its elevation in the past. The marine samples can give a minimum estimate of sea level, and the terrestrial samples give a maximum estimate of sea level. There are samples that have both upper and lower limits. Data used in this thesis are from an unpublished compilation from A.S. Dyke and T.S. James. Most of them are presented in Dyke (1998), England et al. (2004), England et al. (2000), England (1990), and England (1996). There are in total 1127 relative sea level data that are used to constrain the model. Figures 3.5 and 3.6 show locations of samples I use. Using a smaller region, as presented in Figs. 3.5 and 3.6, is important for comparing calculated RSL with observations, which leads us to create a better reconstruction. Because the RSL is calculated in each constraint location, it is better to have a limited number of constraints in each plot. However, it is not possible to simultaneously fit all the minimum and

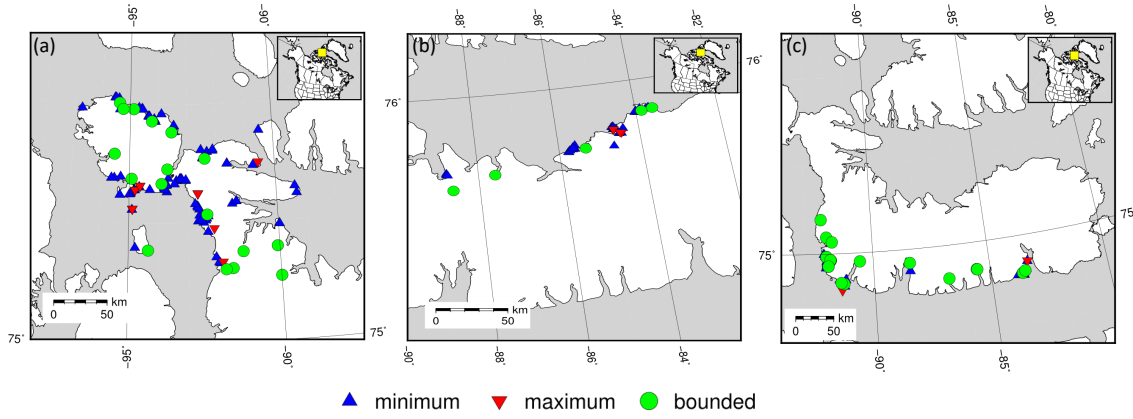


Figure 3.5: Location of relative sea level constraints used in this study on Devon Island. a) Northwest part, b) north part, c) south part [Dyke, 1998; England et al., 2004, 2000; England, 1990, 1996].

maximum in some time steps, which is explained more in Chapter 4. To assess the fit of RSL, a score is added for each meter of disagreement between calculated and observed sea level. For instance, for samples that indicate minimum RSL, if the calculated sea level is below its elevation, for each meter discrepancy program add one to the score, and then add all of the score samples together. The goal is minimizing the score in each sub-region. The ideal fit should have zero score, which is not common in most of regions mainly due to disagreement between some of the data.

### 3.3 Elevation Correction

The desired output of the ICESHEET program is elevation. This elevation is used for correcting  $\delta^{18}\text{O}$ . When the elevation of that location changes over the thousands of years, the obtained  $\delta^{18}\text{O}$  requires correction. I want to reference the  $\delta^{18}\text{O}$  record to a constant elevation. So, the correction brings them to a constant elevation. In this project, I use modern day elevation as a reference and correct the data to this.

To do so, a relation between  $\delta^{18}\text{O}$ -elevation and temperature is needed. The ratio between  $\delta^{18}\text{O}$  versus temperature and temperature versus elevation are estimated in different studies [Dansgaard and Gundestrup, 1973; Johnsen et al., 1989; Cuffey et al., 1995]. The linear relation between temperature and  $\delta^{18}\text{O}$  is  $\delta^{18}\text{O} = aT +$



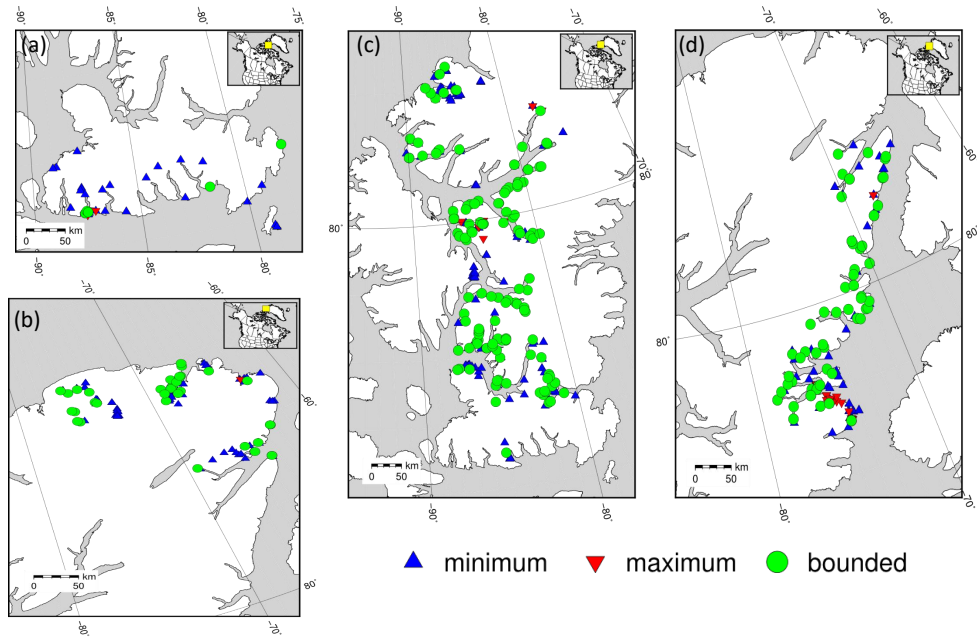


Figure 3.6: Location of relative sea level constraints used in this study on Ellesmere Island. a) South part, b) north part, c) west, d) east [Dyke, 1998; England et al., 2004, 2000; England, 1990, 1996].

*b.* In Greenland, it was estimated, by Dansgaard and Gundestrup (1973) to be  $0.62\text{‰}\text{ }^{\circ}\text{C}^{-1}$ , while Johnsen et al. (1989) obtained value of  $0.67\text{‰}\text{ }^{\circ}\text{C}^{-1}$  for the present time. However, Cuffey et al. (1995) gained different values for  $\delta^{18}\text{O}$  through the time.

*a* is estimated  $\alpha$  to be  $0.33\text{‰}\text{ }^{\circ}\text{C}^{-1}$  before 8 ka, and  $0.25\text{‰}\text{ }^{\circ}\text{C}^{-1}$  for the late Holocene. As a general estimate, the lapse rate is assumed to be  $6\text{ }^{\circ}\text{C km}^{-1}$ . For applying these corrections to the Northern Canadian ice cores, I assume the relation between  $\delta^{18}\text{O}$  and temperature is spatially and temporally constant.

### 3.3.1 ECHAM-wiso

The relation of  $\delta^{18}\text{O}$  to elevation can also be calculated by using models. I use results of model ECHAM5-wiso for present time [Butzin et al., 2014], as one of the accurate models with the high resolution. ECHAM5-wiso is isotope-enabled atmospheric general circulation model, which is explicitly simulating the stable water isotope cycle for present time [Werner et al., 2011]. Butzin et al. (2014) applied ECHAM5-wiso to explore  $\delta^{18}\text{O}$  variations. The horizontal grid size is approximately  $1.1^{\circ} \times$

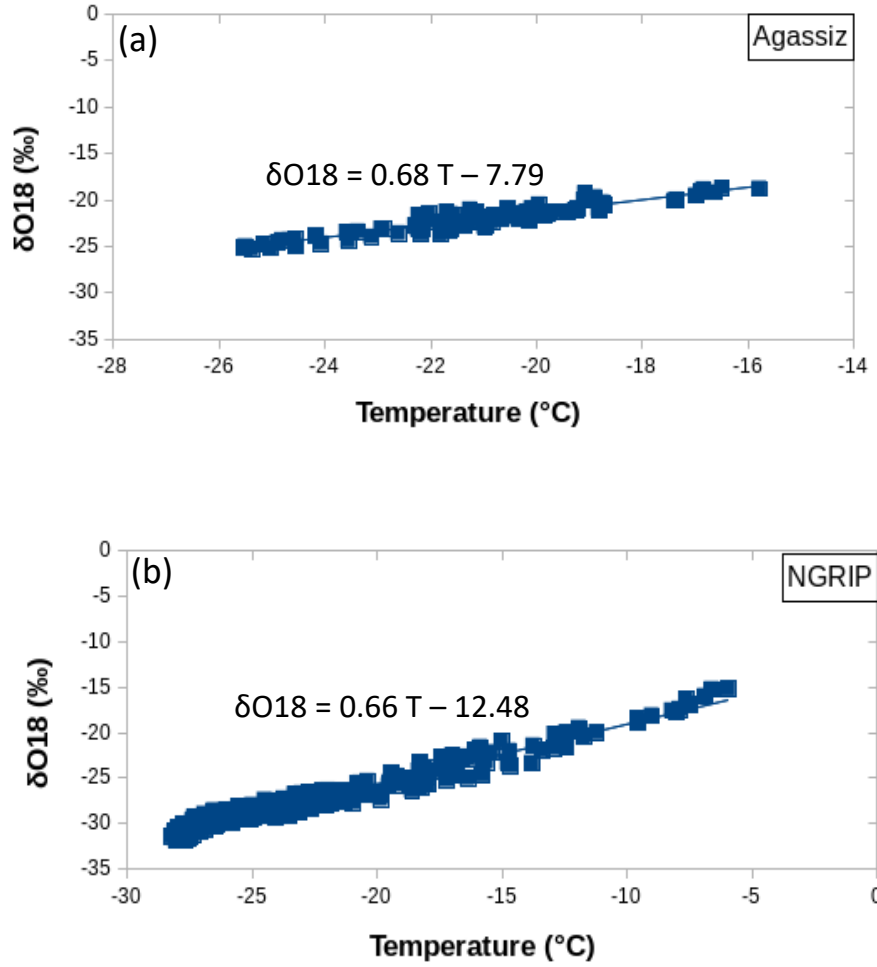


Figure 3.7: The relation of  $\delta^{18}\text{O}$  to temperature on the base of ECHAM5-wiso. a) 85 data points from Ellesmere and Devon Island with correlation coefficient of 0.94, b) 206 data points from the middle of Greenland Ice Sheet with correlation coefficient of 0.98 [Butzin et al., 2014].

1.1°. The  $\delta^{18}\text{O}$  versus temperature and elevation are presented in Figs. 3.7 and 3.8, respectively. The slope of linear fitted line to  $\delta^{18}\text{O}$ -temperature are approximately the same, while the slope of fitted line between  $\delta^{18}\text{O}$ -elevation at the Agassiz ice core is  $\frac{3}{2}$  of the same at NGRIP. To obtain the relation between  $\delta^{18}\text{O}$  versus temperature and elevation for the Agassiz Ice Cap, the data of 85 grid point are used. This covers Ellesmere and Devon Island. 206 grid points in Greenland are used to determine same relations there. The least square method is applied for a linear fit to each plot. The correlation coefficient between  $\delta^{18}\text{O}$  and temperature is 0.94 for the Agassiz

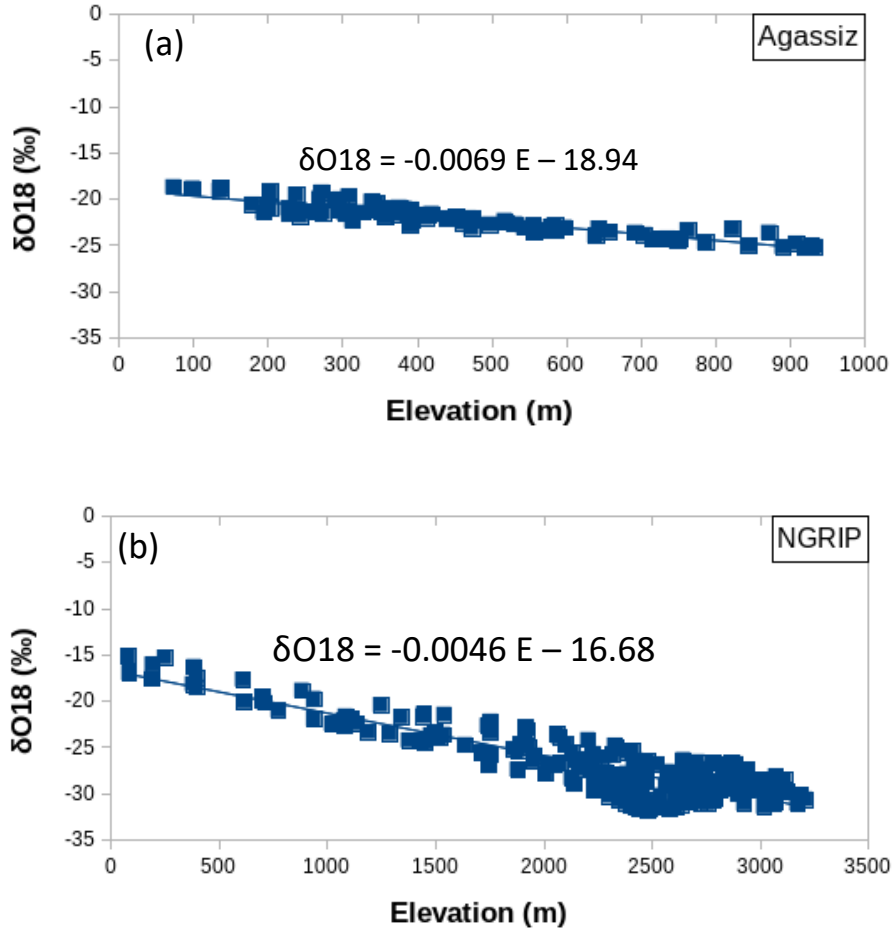


Figure 3.8: The relation of  $\delta^{18}\text{O}$  to elevation on the base of ECHAM5-wiso. a) 85 data points from Ellesmere and Devon Island with a correlation coefficient of -0.917, b) 206 data from the middle of Greenland Ice Sheet with a correlation coefficient of -0.894 [Butzin et al., 2014].

Ice Cap and 0.98 for NGRIP. The correlation coefficient between  $\delta^{18}\text{O}$  and elevation is -0.917 and -0.894 for the Agassiz Ice Core and NGRIP respectively. The  $\alpha$  is extracted for the Canadian Archipelago and Greenland with the assumption that it is temporally constant.

To convert  $\delta^{18}\text{O}$  to the temperature, I use two different relations. The relation from ECHAM-wiso model, hereafter named ECHAM temperature relation and the relation obtained by Dansgaard and Gundestrup (1973), hereafter named Dansgaard temperature relation. Moreover, the results based on the relation between  $\delta^{18}\text{O}$  and

elevation, calculated by Dansgaard temperature relation based on the lapse rate, is compared to the relation between  $\delta^{18}\text{O}$  and elevation using ECHAM-wiso model (here referred to as Dansgaard elevation relation and ECHAM elevation relation, respectively).

# Chapter 4

## Results and Discussion

### 4.1 Ice Sheet Reconstruction

The method I am using to do the Innuitian Ice Sheet reconstruction is independent of climatic variables such as temperature and precipitation. This make it useful for climate and ice sheet dynamics modelling as an independent input. There is a sequence of steps to calculate ice thickness and surface elevation with the ICESHEET program. The ice sheet is calculated first, using three inputs (ice margin, topography, and shear stress) as described in Chapter 3. Calculation of the Earth's surface deformation using the reconstructed ice sheet (GIA) is the next step. The calculated sea level is obtained over thousands of years relative to present time. The 1127 regional relative sea level observations are used as a constraint for improving the reconstruction. Finally, the shear stress of sub-regions is adjusted and the steps are repeated to reach the final reconstruction, which will be presented in this chapter. These are combined with the to original reconstruction of [Gowan et al. \(2016a,b\)](#).

#### 4.1.1 Relative Sea Level

The Agassiz and Devon Ice Caps are the main focus in this study, which are on Ellesmere and Devon Islands, respectively. The results of two islands are shown separately. For each island, the sea level is constrained by dividing them into smaller regions as shown in Figs. 3.5 and 3.6. I show the sea level calculated at all of the samples' location after reconstruction. Two kinds of plots are used to evaluate the

agreement between calculated sea level and observations (Figs. 4.1 to 4.3). On the basis of these two plots in each region I decided to increase or decrease the ice thickness by adjusting shear stress. In the most of regions the modelled sea level was initially too low, which means the ice sheet needed to be thicker. When thicker ice was needed, I increased the shear stress in that region and its vicinity. Sometimes, changing shear stress in surrounding regions was also required.

The plots on the left side of Fig. 4.1 to Fig. 4.3 show actual calculated sea level with sea level constraints. The sea level is calculated at the location of each sample. The time scale of each plot has been chosen to include the oldest samples in the sub-region. A variety of sea level responses in the sub-regions can be seen in these plots. Violated constraints cannot be easily distinguished based on these plots. In all regions, except in northwest of Devon Island, a great variety of sea level responses can be seen in the sub-regions. Variety of sea level responses in small regions is the reason to use all sea levels constraint for fitting the sea level.

Where there is a wide variety of sea level responses, like in the south of Ellesmere Island, a metric is needed to define whether the fit improved or not. This metric is the score, which is written in the top right corners of the plots. The minimum sea level constraints, for instance, are satisfied when the elevation of the calculated sea level curve is above it. In this case, the score is zero. The number of meters the sea level curves is below the minimum constraints are added to the score. The overall score is the sum of all individual observation samples in the regions. Consequently, when the number of samples in the region is high, it is more likely to have high score. The difference between elevation of samples and calculated sea level is shown in the plots on the right side of the figures. In an ideal case, all minimum constraints (blue one) should be below zero, and maximum (red) above zero. The bounded constraints should be on the zero line. In Devon south, for example, all of minimum constraints are satisfied. The high score is mainly because of bounded constraints that do not fit.

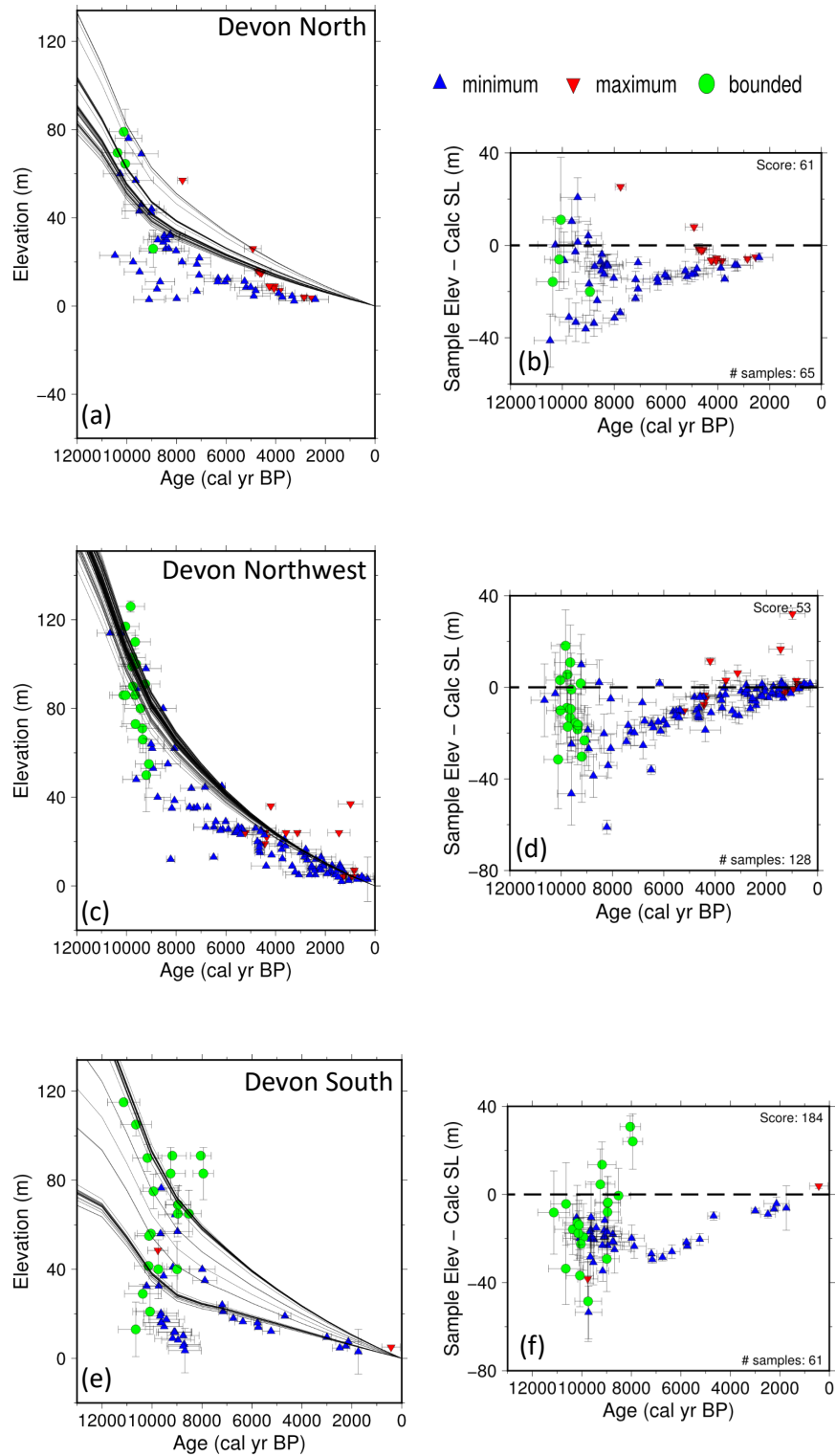


Figure 4.1: Devon Island. a,c,e) different between relative sea level constraints and calculated one; b,d,f) relative sea level constraints and calculated sea level in north, northwest and south respectively.

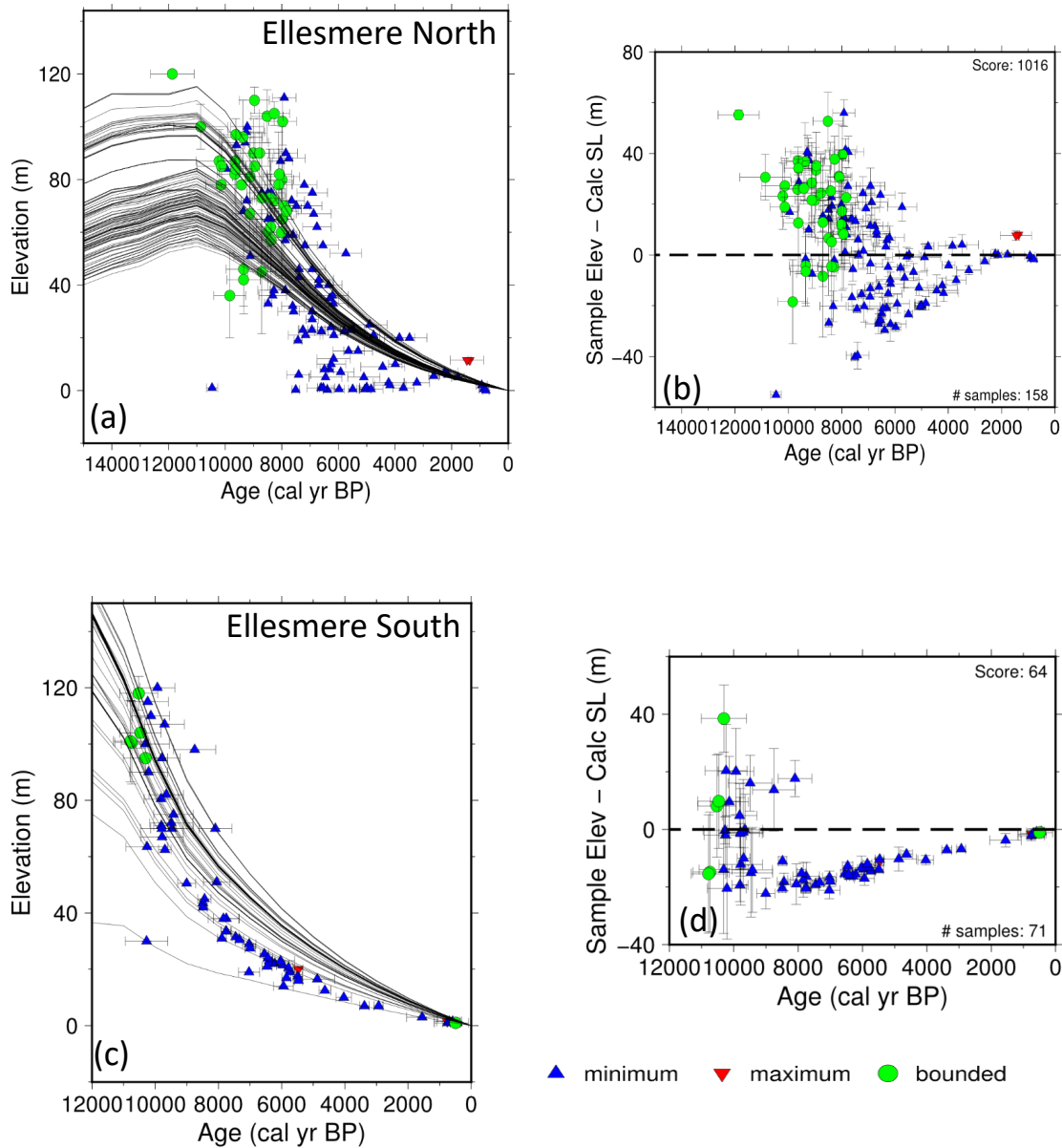


Figure 4.2: Ellesmere island, a,c) different between relative sea level constraints and calculated one; b,d) relative sea level constraints and calculated sea level in north and south respectively.

The Devon Island sea level constraints fit quite good, as shown in Fig. 4.1. In the north of Ellesmere Island, the constraints older than 6 ka do not fit well, which may indicate the ice sheet need to be thicker before 6 ka in this region. To satisfy the constraints, in eastern of Ellesmere Island, the actual sea level curves should be steeper. This could be accommodated by decreasing the mantle viscosity. Lowering the mantle viscosity causes a faster response of the Earth's crust [James et al., 2009]. I did not change the mantle viscosity because the calculated sea level in



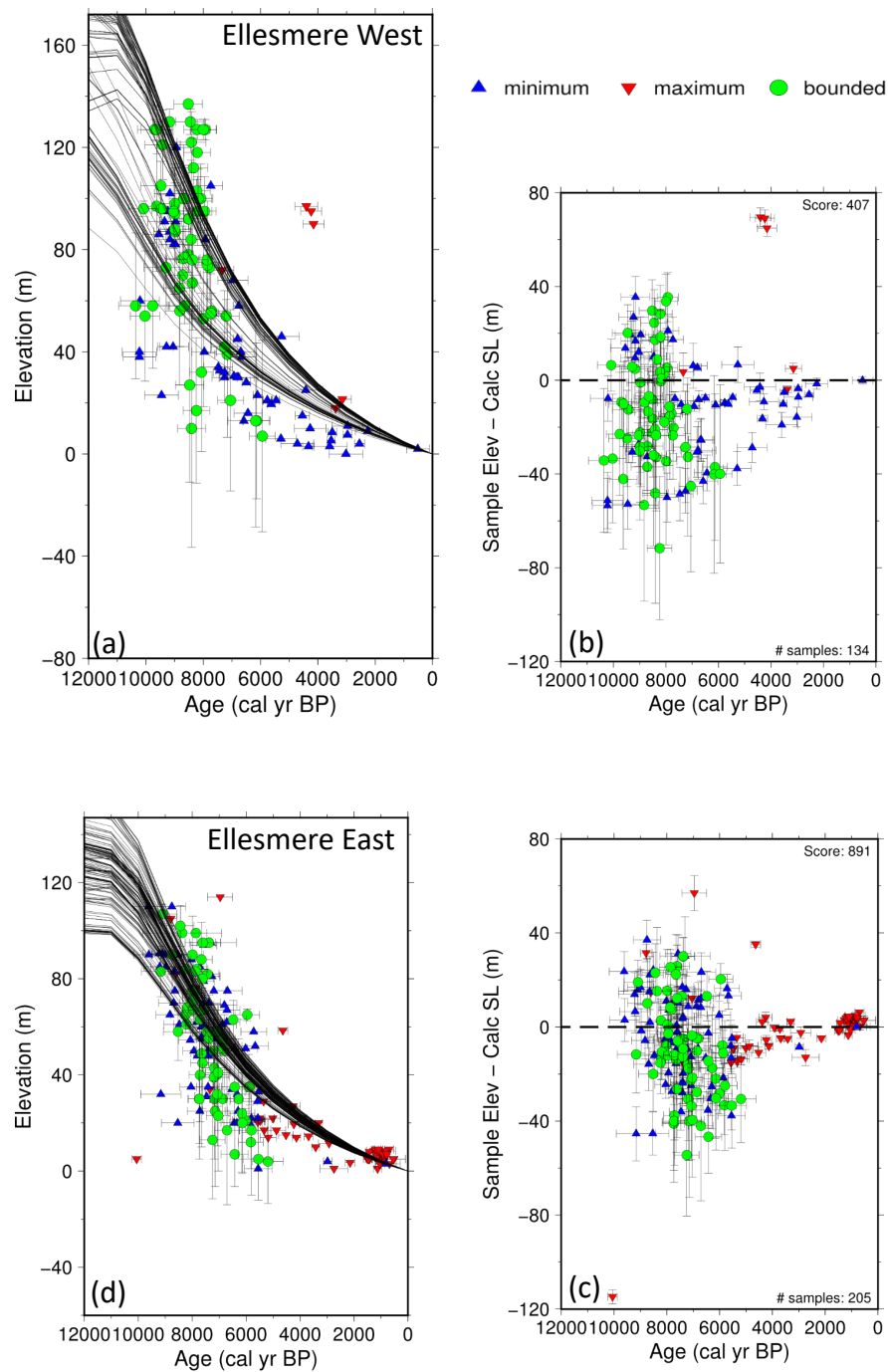


Figure 4.3: Ellesmere Island, a,c) different between relative sea level constraints and calculated one; b,d) relative sea level constraints and calculated sea level in west and east respectively.

other regions were seemed consistent with the data and changing it will influence the whole region significantly.

### 4.1.2 Elevation and Ice Thickness

The thickness of the reconstructed ice sheet with 5000 year intervals is shown in Fig. 4.4. Elevation change is presented with the same interval on Fig. 4.5. The locations of domes have good agreement with England et al. (2006). During the Last Glacial Maximum, the elevation was less than ice thickness in that region. This means weight of ice sheet pressed the Earth's surface down. However, the elevation is higher during the retreat period, which is due to the rebound of the Earth's surface.

The major difference is between 15 ka (Fig. 4.5d) and 5 ka (Fig. 4.5b). Other intervals do not significantly vary. The retreating of the Innuitian Ice Sheet with higher temporal resolution in thousands of years is illustrated on Fig. 4.6 and Fig. 4.7, which shows the ice thickness and surface elevation respectively. The maximum elevation of the Innuitian Ice Sheet is about 3200 m in this reconstruction at 20 ka, which is higher than in ICE-6G (2500 m). In ICE-6G (Fig. 2.3 and Fig. 2.1) there is no change in ice thickness and elevation between 20 and 25 ka. Evidence from the ice margin reconstruction shows advance of ice sheet between 30 ka to 23 ka [England et al., 2000; England, 1999; England et al., 2004]. This ice sheet advance can be seen in Fig. 4.4, Fig. 4.5, and Fig. 3.3.

## 4.2 Correction of $\delta^{18}\text{O}$

As explained in Chapter 3, to correct  $\delta^{18}\text{O}$ , elevation change of the ice cap is needed. The elevation from the reconstruction are originally presented in a 5 km  $\times$  5 km resolution grid. To avoid local topographic variations, I averaged elevation over 16 grid cells (20 km  $\times$  20 km). This is presented in Fig. 4.8.

### 4.2.1 Agassiz Ice Cap

The advance and retreat of the Innuitian Ice Sheet can be seen in elevation changes of Agassiz Ice Cap (Fig. 4.8a). There is a gradual decrease from maximum height at

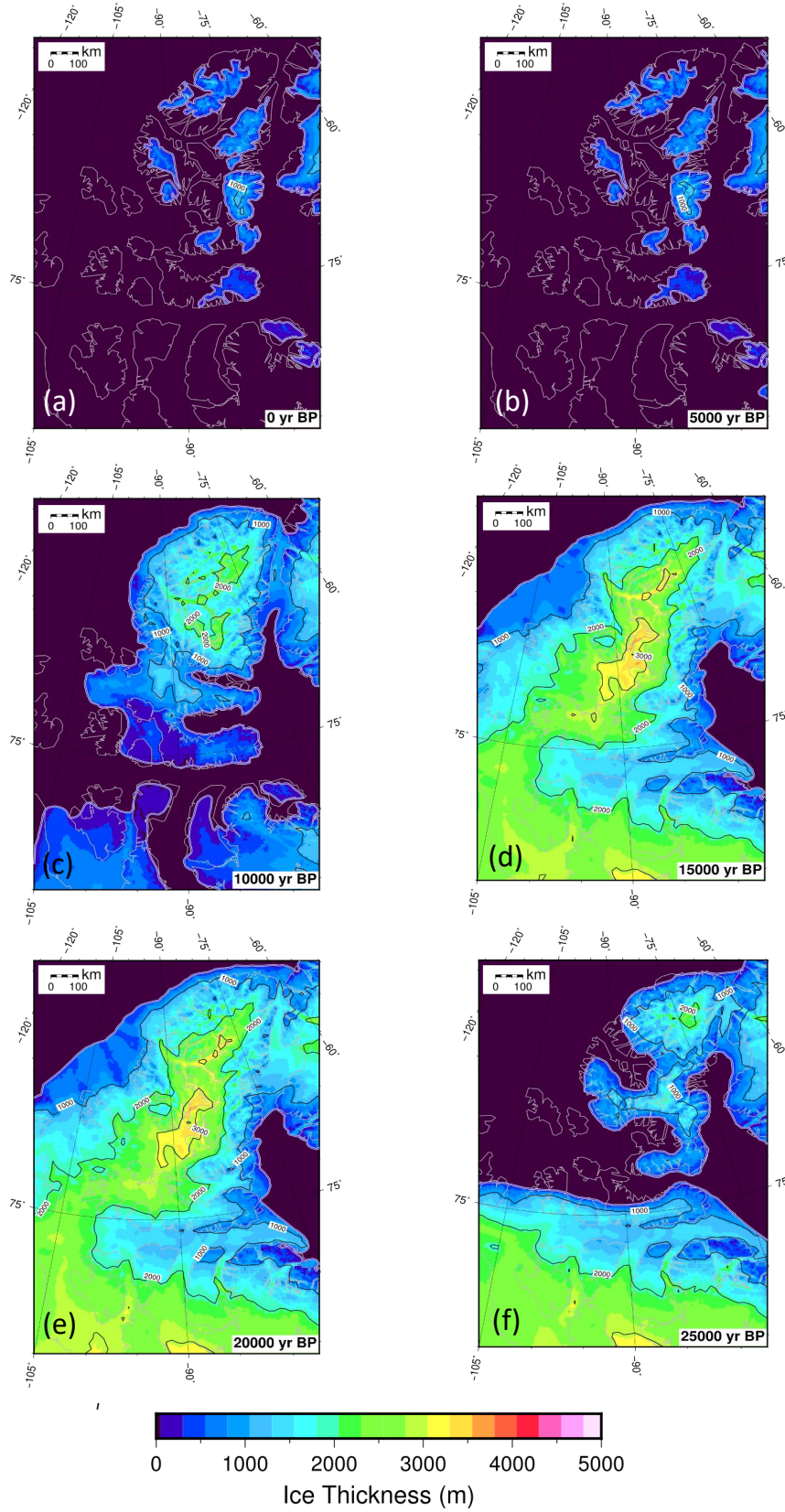


Figure 4.4: The Innuitian Ice Sheet ice thickness (in meters) from LGM to Present using the ICESHEET program[Gowan et al., 2016b,a].

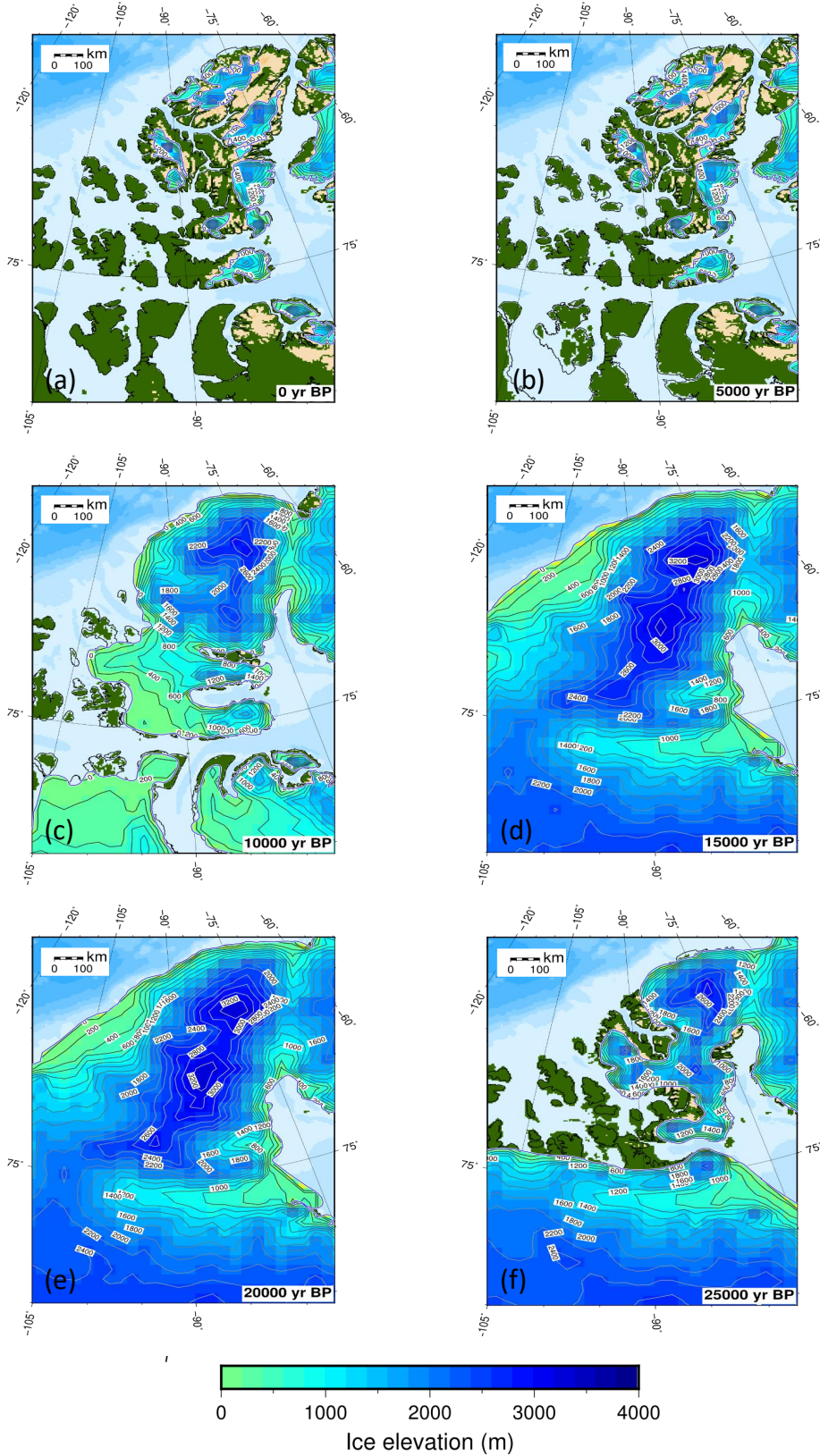


Figure 4.5: The Innuitian Ice Sheet surface elevation (in meters) from LGM to Present using the ICESHEET program[Gowan et al., 2016b,a].



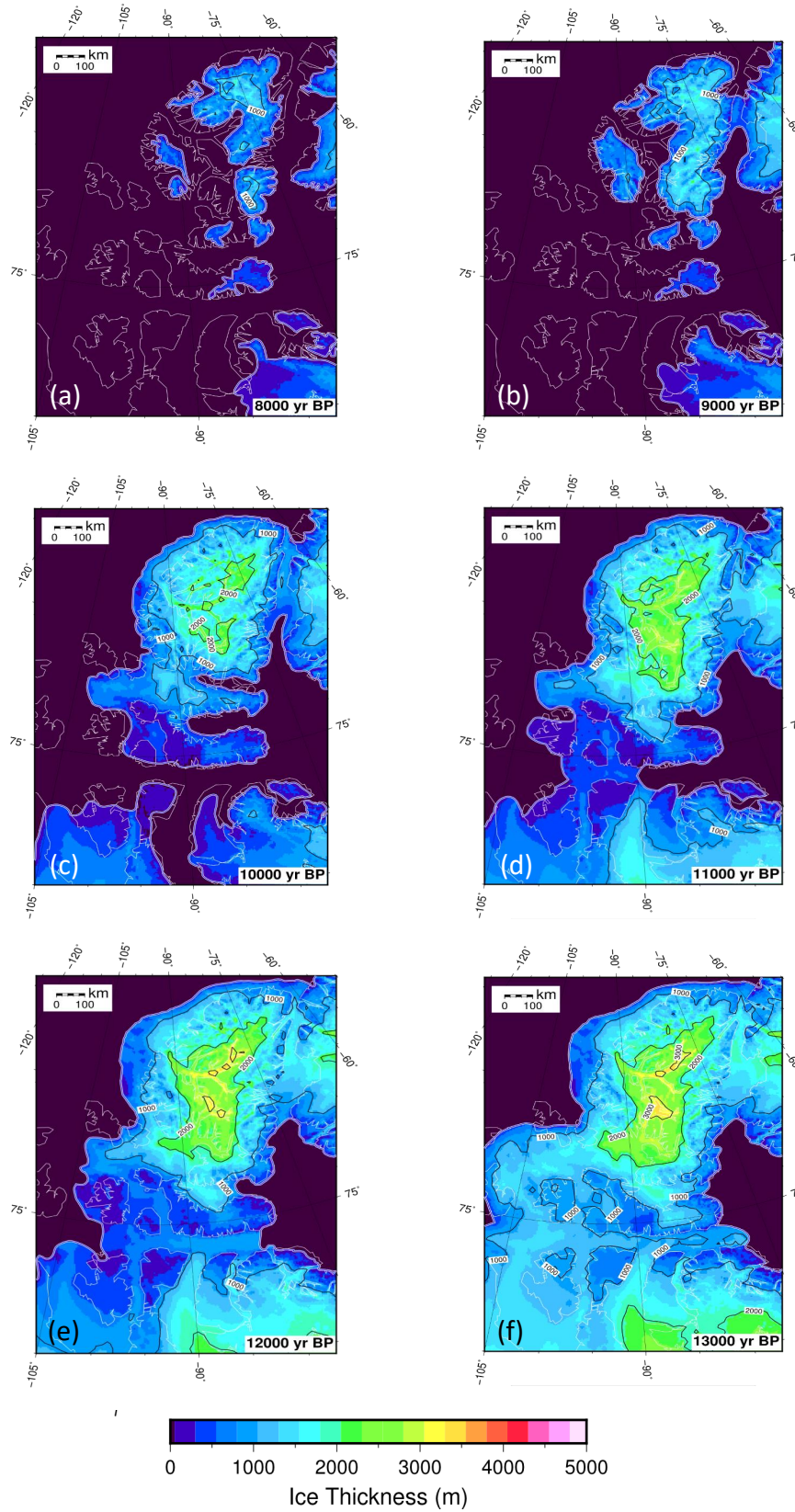


Figure 4.6: As Fig. 4.6 but over retreat time from 13 ka to 8 ka.

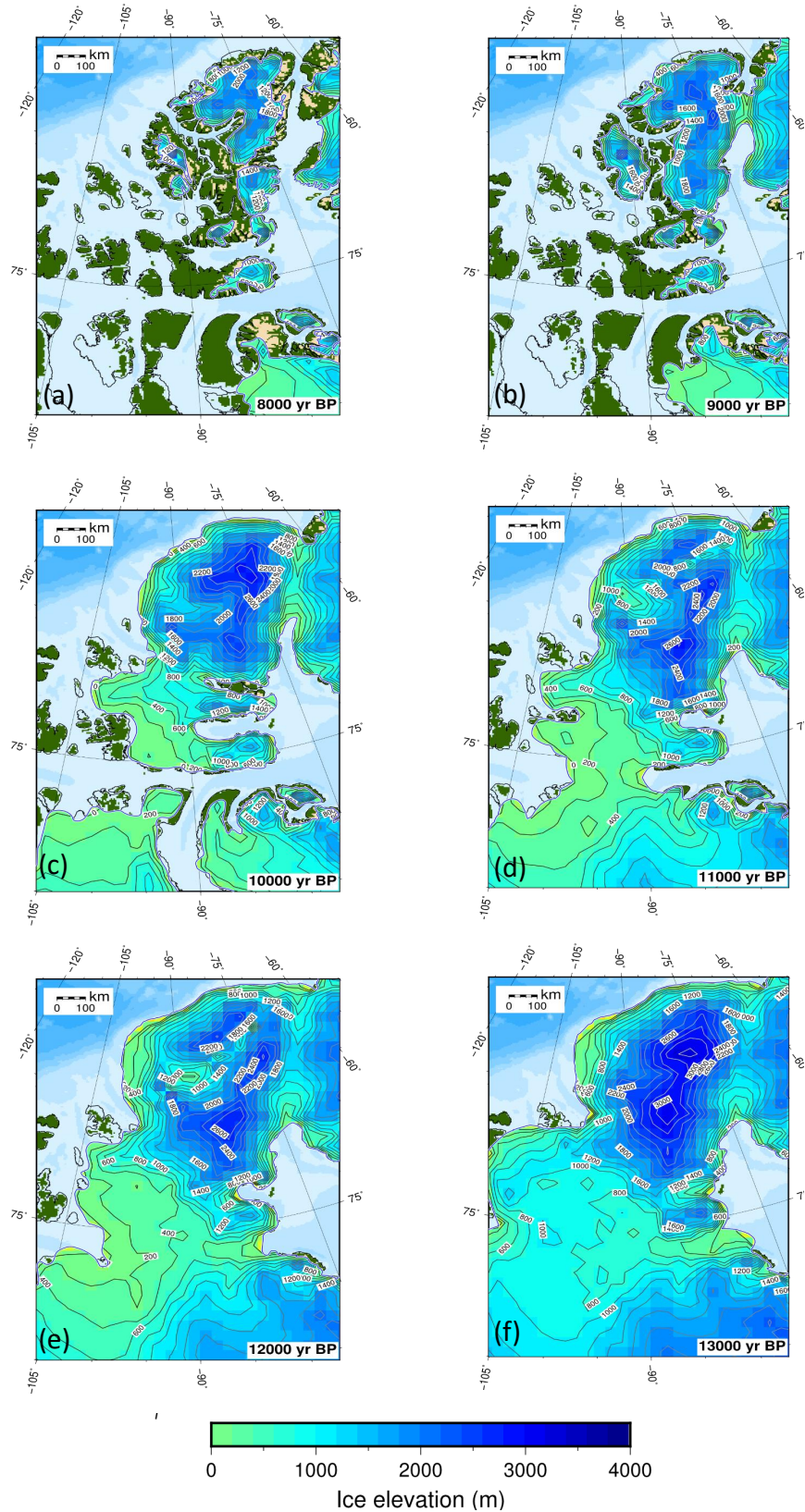


Figure 4.7: As Fig. 4.5 but over retreat time from 13 ka to 8 ka.

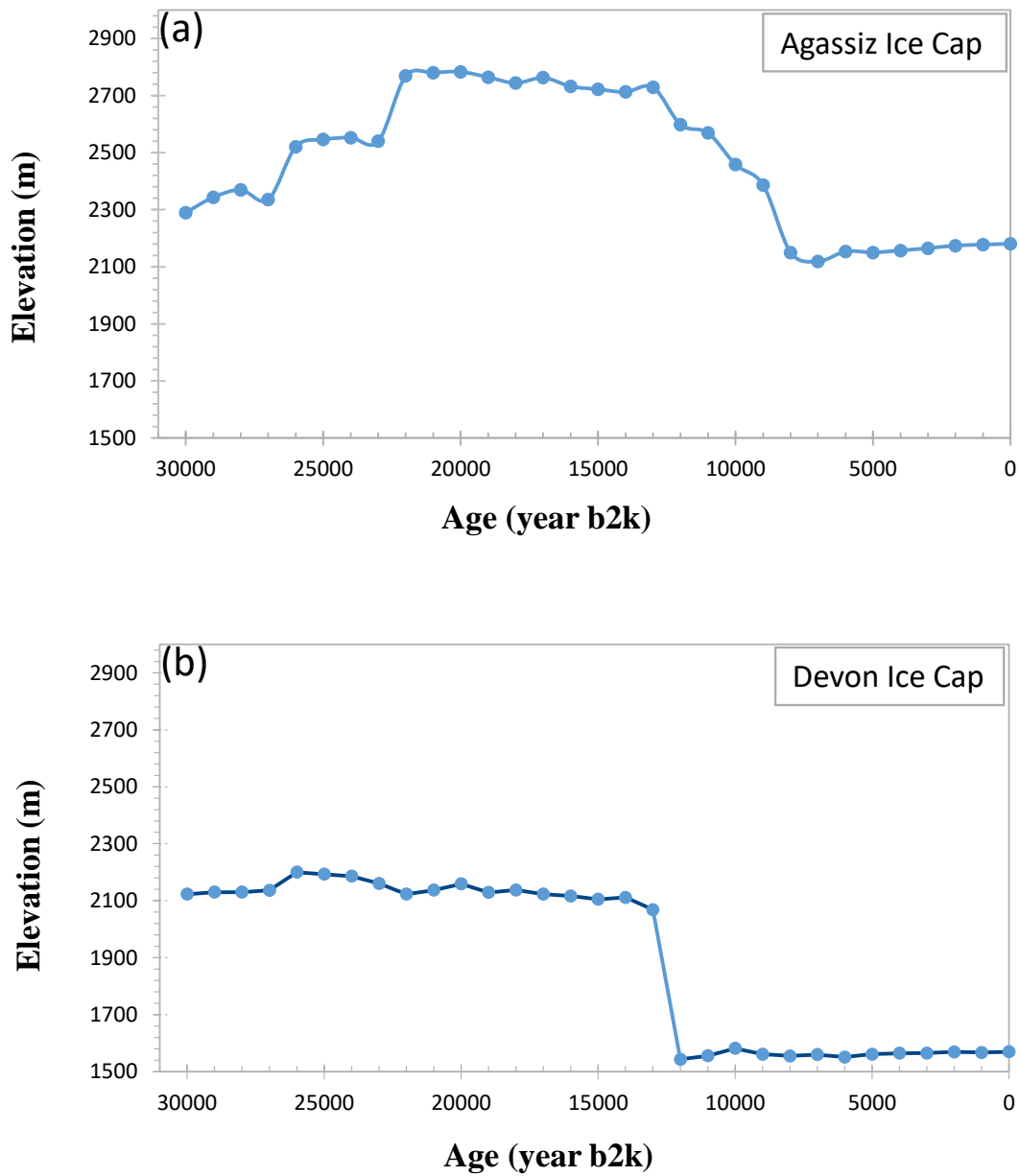


Figure 4.8: Surface elevation of a) the Agassiz (80.7 °N, 73.1 °W), b) the Devon ice cap (75.34 °N, 82.17 °W) based on the ICESHEET reconstruction [Gowan et al., 2016b,a].

22 ka to 8 ka. The ice margins do not change between 22 ka to 13 ka, so the elevation decrease slightly over these time. Because it takes a while for mantle to response to the ice sheet, when the ice sheet growth stops (constant ice thickness), the surface elevation decreases because of the Earth's surface deformation. However, between 13 ka and 8 ka due to the retreat of ice margins the elevation falls dramatically.

The influence of the Innuitian Ice Sheet advance is also clear between 30 ka and 22 ka. The first significant changes happened between 27 and 28 ka, when the ice of the northern and eastern parts on Ellesmere Island coalesced. The second stage is due to the growth of the margin to the east and west of Agassiz Ice Cap (between 23 ka and 22 ka). The growth to the east and west of Ellesmere Island influenced elevation of the site more than changes in the northern extent of the ice sheet.

The general pattern of retreat in my reconstruction and ICE-6G reconstruction is similar from 20 ka to present. In ICE-6G, the reduction of elevation is higher (Fig. 2.3). The elevation of Agassiz decreases about 900 m between 13 ka and 8 ka, while in my reconstruction it is reduced by 520 m between 14 ka and 8 ka. However, the elevation range in ICE-6G is from 2200 m to 1300 m, which is less than my reconstruction (2700 m to 2200).

Although the  $\delta^{18}\text{O}$  correction on the base of my reconstruction is less than ICE-6G, it is still indicate higher early Holocene temperature, which is shown in Fig. 4.9 to Fig. 4.12. As it is explained in Chapter 3, There are four Agassiz ice cores. Two of them are from the dome (A84 and A87) and other two are south and southwest of the dome (A77 and A79 respectively). The trend of  $\delta^{18}\text{O}$  for each of them with and without the correction are presented in separate figures (Fig. 4.9 to Fig. 4.12). The "a" plots shows correction based on the Dansgaard temperature relation.

$$\delta^{18}\text{O} = \alpha T + b$$

where  $\alpha$  and  $b$  are  $0.62 \text{‰ } ^\circ\text{C}^{-1}$  and  $-15.25 \text{‰}$ , respectively.

the ratio between  $\delta^{18}\text{O}$  and elevation is obtained with:

$$\frac{0.62 \text{‰}}{1^\circ\text{C}} \times \frac{6^\circ\text{C}}{1000\text{m}} = 0.00372 \text{‰m}^{-1}$$

The second plots (b) show the correction based on ECHAM5 elevation relation [Butzin et al., 2014], which is shown in Fig. 3.8. The ratio between  $\delta^{18}\text{O}$  and elevation is  $0.0069 \text{‰ m}^{-1}$  which is almost double that of the Dansgaard elevation



relation.

Regardless of correction, the early Holocene climatic optimum is pronounced. It happened in the original  $\delta^{18}\text{O}$  record between 10 ka to 9 ka. The correction based on the Dansgaard elevation relation increases  $\delta^{18}\text{O}$  at 11.7 ka by 1.32‰, which corresponds to a 2.14 °C rise in temperature. The ECHAM correction is higher, and gives a temperature increase of 3.64 °C due to a 2.46‰  $\delta^{18}\text{O}$  increase. The corrections result in an earlier peak temperature, especially in A79 (Fig. 4.11). These results consistent with [Lecavalier et al. \(2017\)](#)'s results. They found the discrepancy between temperature reconstruction of the isotope data ( $\delta^{18}\text{O}$ ) and ice melt percentage [[Fisher et al., 2012](#)] in the Agassiz ice core declines when applying elevation corrections. Because the Agassiz melt records have an earlier temperatures peak than the original temperature reconstruction of  $\delta^{18}\text{O}$ .

#### 4.2.2 Devon Ice Cap

Devon Ice Cap experienced less elevation variability than Agassiz. There are two levels of elevation (Fig. 4.8) with a transition time of 1000 years. Elevation decreases dramatically between 13 ka and 12 ka (540 m). Compared to ICE-6G, elevations are higher in all steps. Devon has a maximum elevation of 1460 m, which is almost constant from 20 ka to 15 ka (Fig. 2.3). The elevation decreases 150 m in total during this time interval. The elevation in my reconstruction is 1570 m at present time and the maximum is 2110 m at 20 ka.

As shown in Fig. 3.2, the bottom of Devon ice core is not reliable, so we can only trust and correct the past 10000 years. During this period, the elevation remains constant. This means there is no need of a correction in the Devon ice core.

### 4.3 Greenland

In this thesis the Innuitian Ice Sheet was reconstructed with ICESHEET program. There is no attempt to make a Greenland reconstruction and model sea level. In

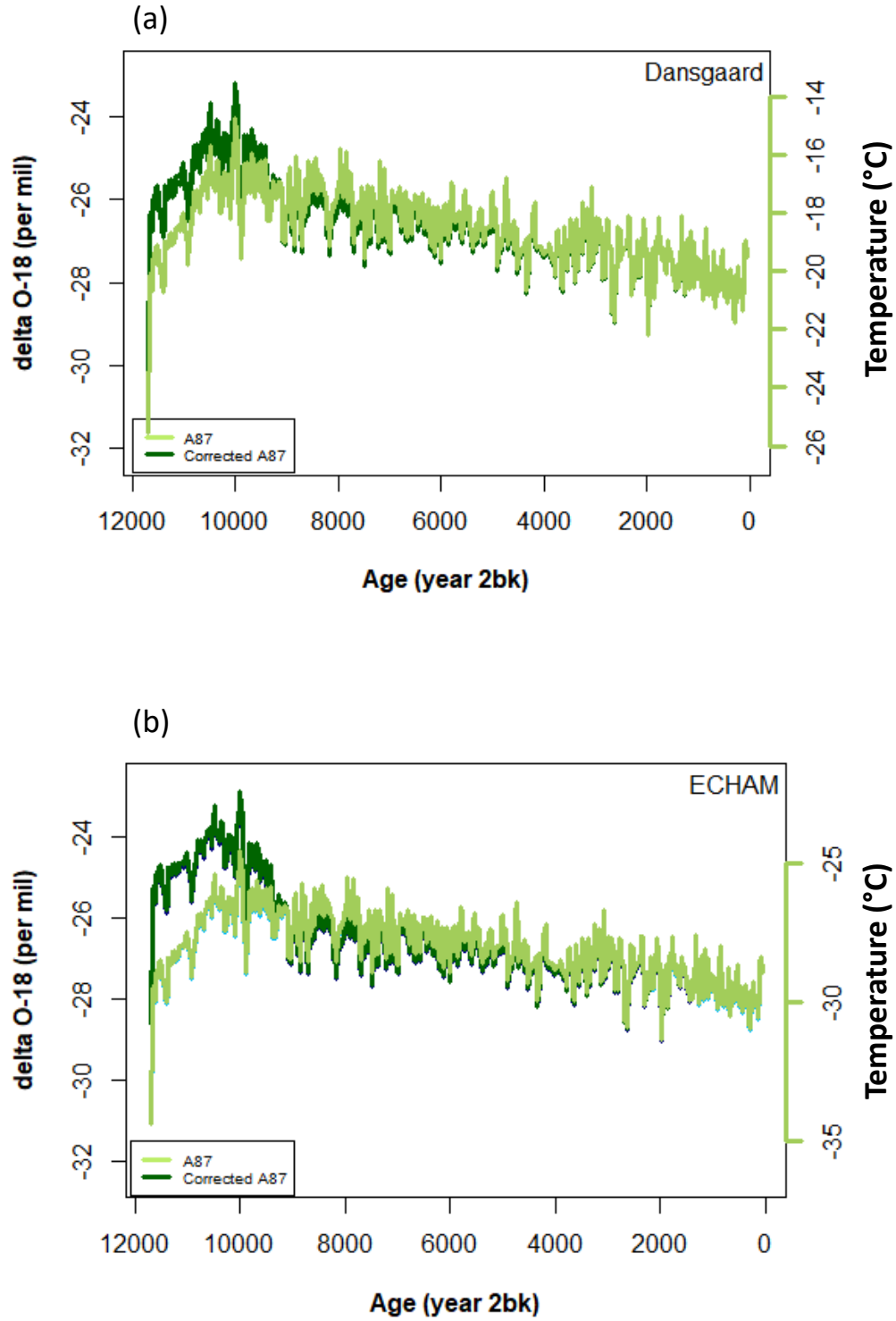


Figure 4.9: Agassiz  $\delta^{18}\text{O}$  data of ice core A87 on the GICCO5 timescale with and without correction (dark and light green respectively). Corrections are based on a) [Dansgaard and Gundestrup \(1973\)](#) relation between  $\delta^{18}\text{O}$  and temperature b) ECHAM model data between  $\delta^{18}\text{O}$  and elevation.

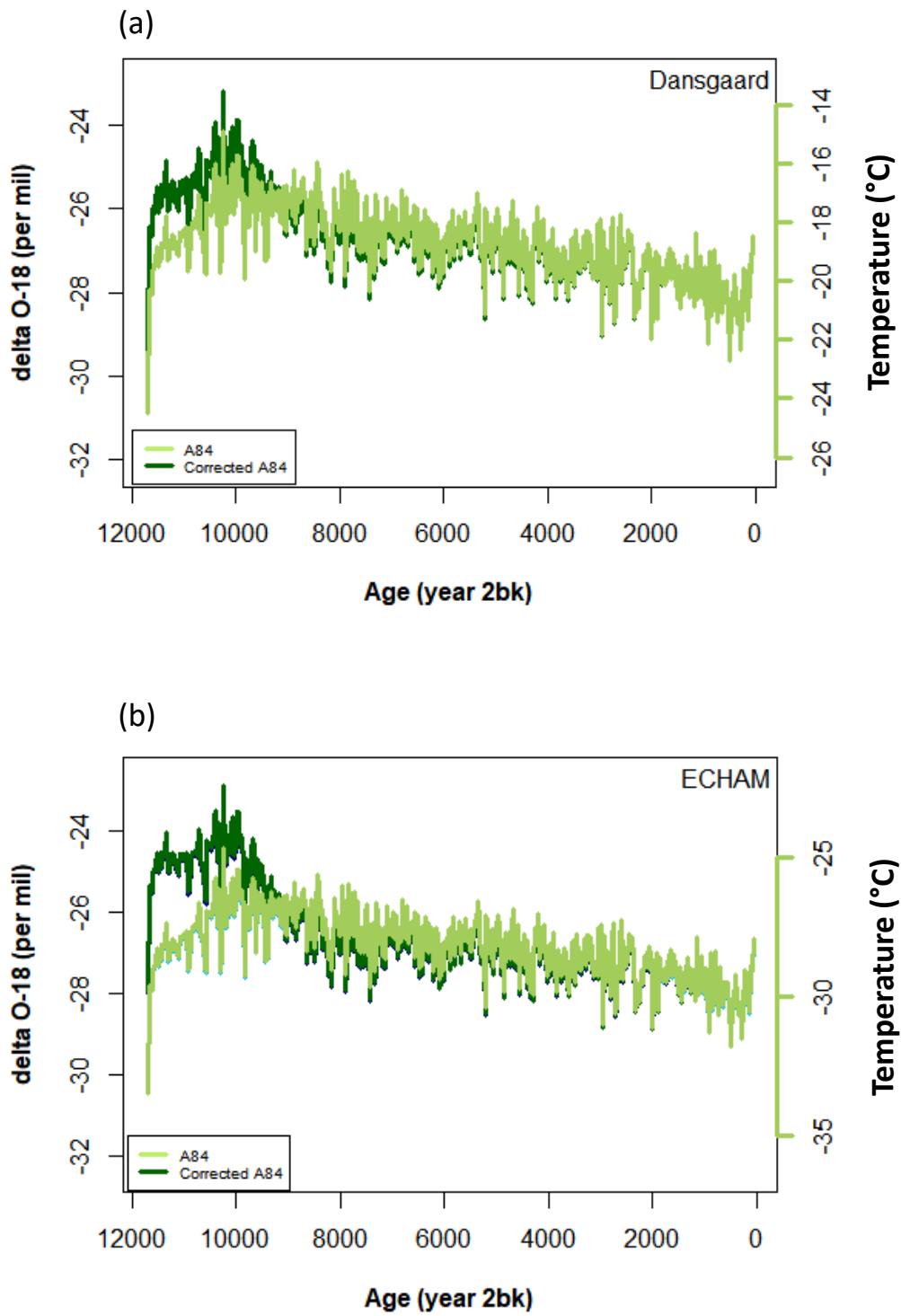


Figure 4.10: As Fig. 4.9 but for A84.

this section, I am going thorough the Greenland history with two different assumptions.

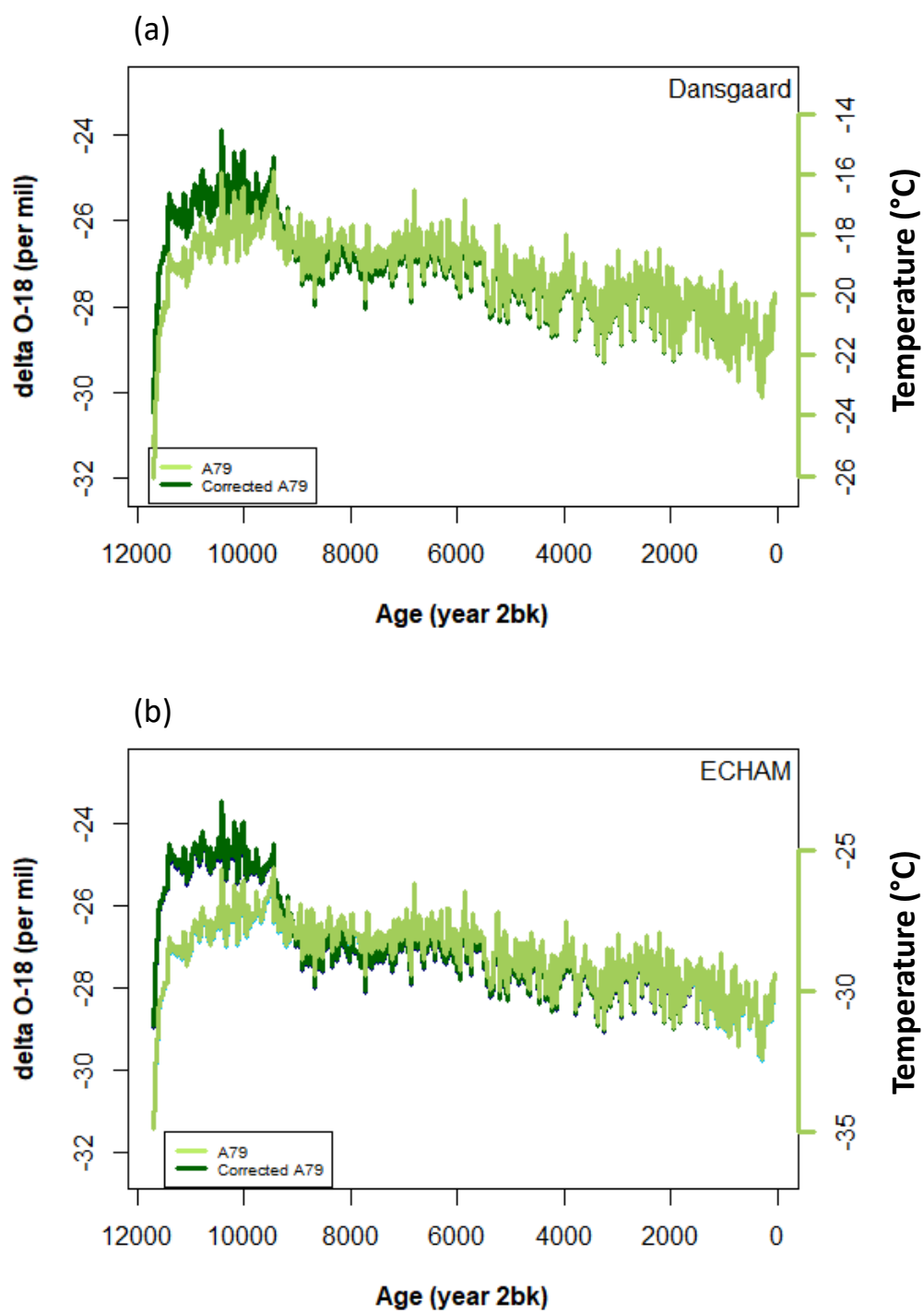


Figure 4.11: As Fig. 4.9 but for A79.

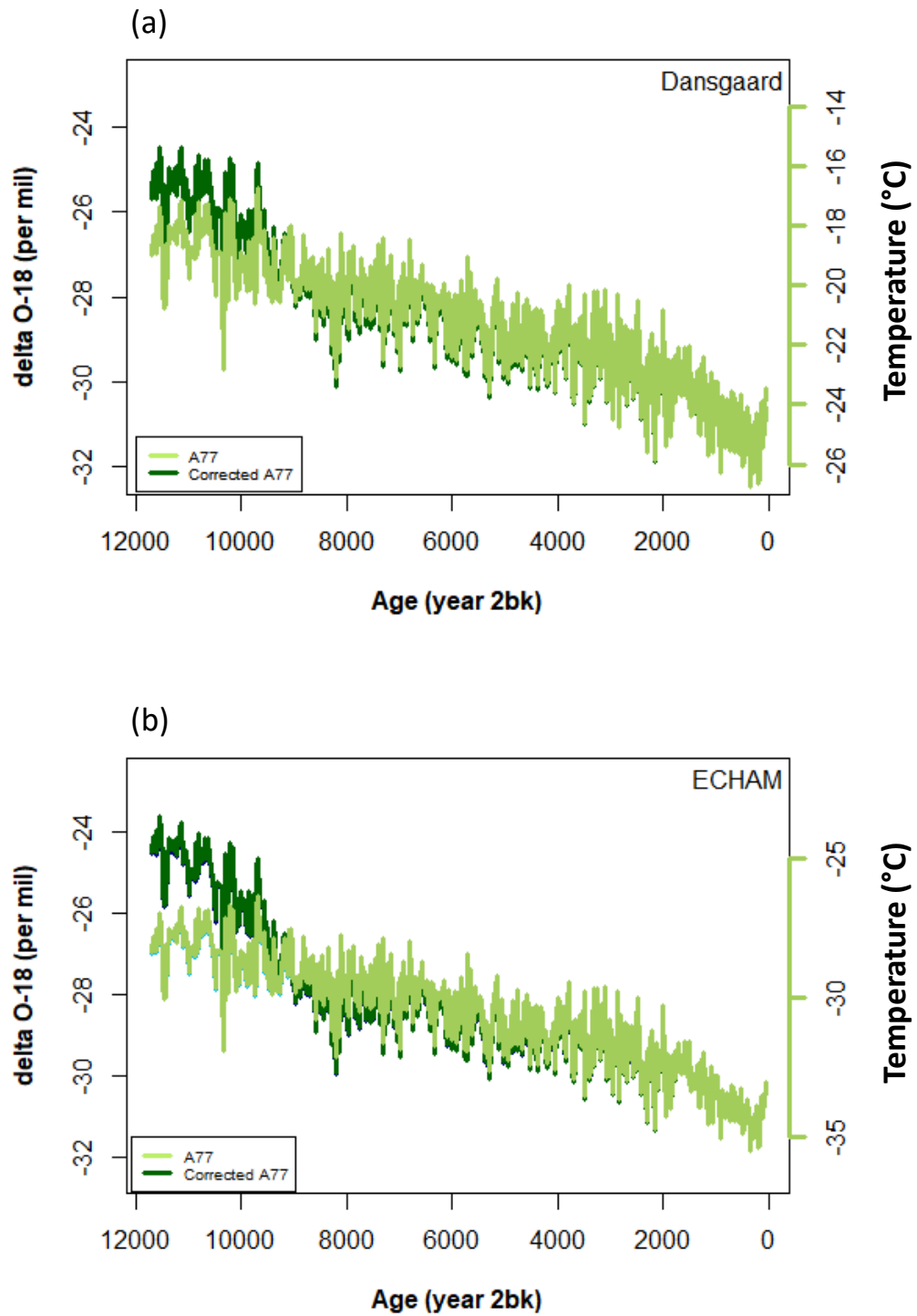


Figure 4.12: As Fig. 4.9 but for A77.

#### 4.3.1 Homogeneous Climate

I first follow the method of [Vinther et al. \(2009\)](#) to determine elevation changes in NGRIP. The idea is that the discrepancy between  $\delta^{18}\text{O}$  trends in neighbouring

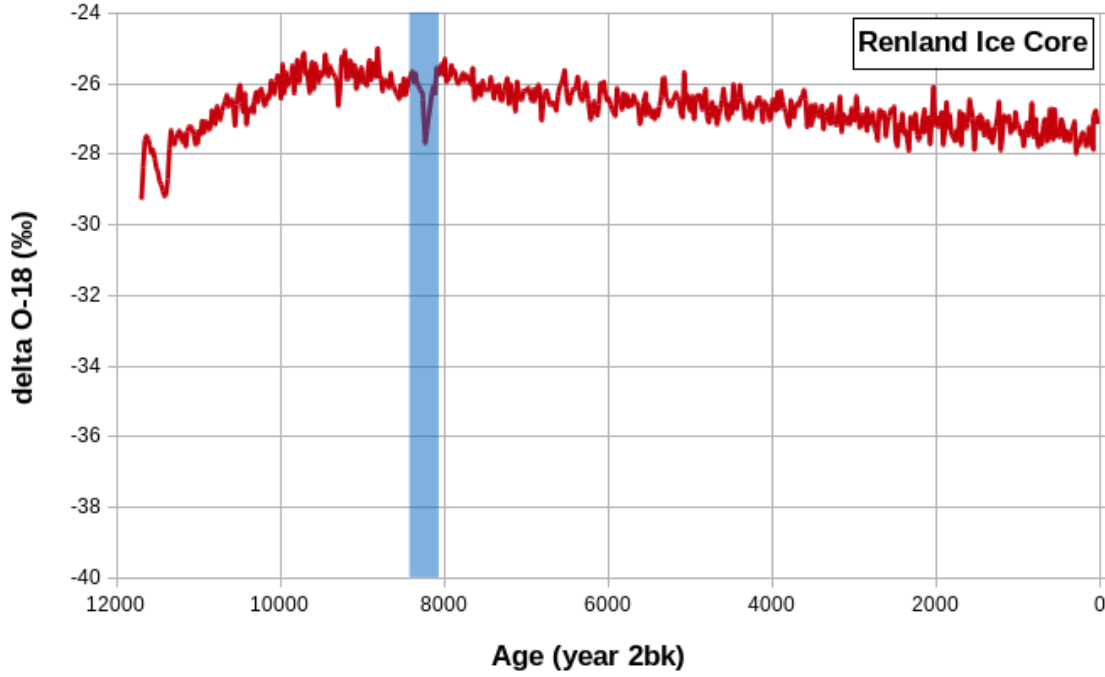


Figure 4.13:  $\delta^{18}\text{O}$  data on GICC05 timescale in Renland Ice Core; blue column illustrate 8.2 ka event [Johnsen et al., 1992b; Vinther et al., 2008].

ice cores are due to past changes in the elevation of the sites. They claim, due to the similarity of  $\delta^{18}\text{O}$  values in the Agassiz and Renland Ice Caps, that the Greenland climate during the Holocene was homogeneous. The Renland  $\delta^{18}\text{O}$  trends are presented in Fig. 4.13. The Agassiz and Renland Ice Caps are separated by 1500 km and by the entire Greenland Ice Sheet, but their  $\delta^{18}\text{O}$  trends are similar. The location of Renland is shown in Fig. 1.1. If the climate was homogeneous during the Holocene, the difference in  $\delta^{18}\text{O}$  records between Agassiz and Greenland are result from changes in elevation between the two sites.

The next step is to convert  $\delta^{18}\text{O}$  to elevation. The Agassiz Ice Cap is used as a reference and NGRIP elevation is obtained on the basis of the Agassiz elevation. The calculated change of NGRIP elevation is shown in Fig. 4.15.

The difference between  $\delta^{18}\text{O}$  records in NGRIP and Agassiz is presented in Fig. 4.14. To reduce noise and have smoother plots, a 400 year averaged filter is used. The

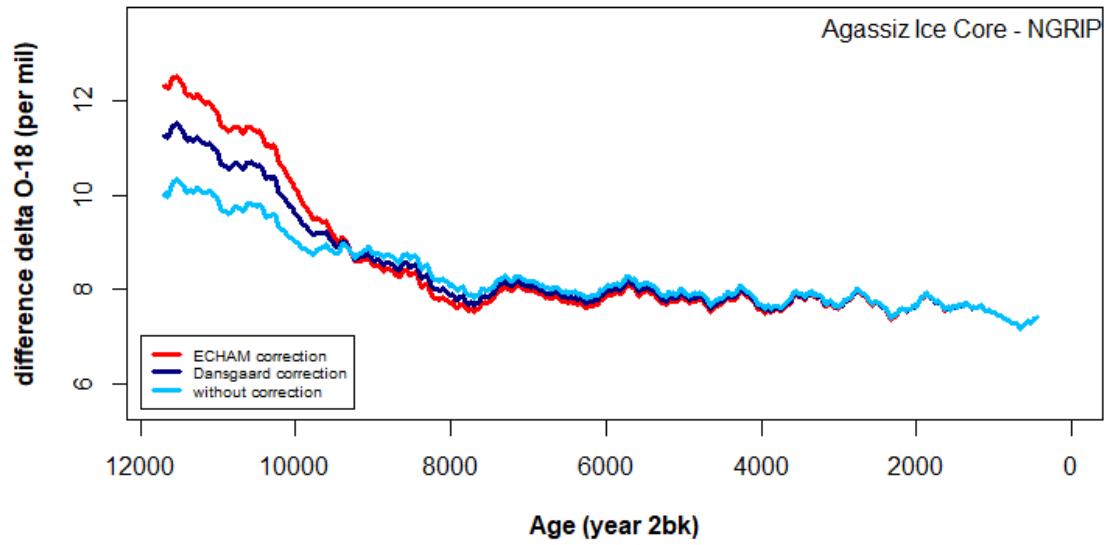


Figure 4.14: Difference of  $\delta^{18}\text{O}$  data between Agassiz ice core (with and without correction) and NGRIP in Greenland.

correction makes the difference in  $\delta^{18}\text{O}$  larger. The Greenland  $\delta^{18}\text{O}$  is less than Agassiz (Fig. 3.1), and the correction increases  $\delta^{18}\text{O}$ , which means it makes the discrepancy larger. The ECHAM elevation relation raises the discrepancy by more than 2 ‰, while it is about 1 ‰ with the Dansgaard elevation relation.

The elevation change at Greenland Ice Sheet varies between 250 m to 800 m when applying different corrections (Fig. 4.15). There are four curves representing elevation changes in NGRIP. The difference between unmodified curves (light blue) shows the influence of the  $\delta^{18}\text{O}$ -elevation ratio between Dansgaard and ECHAM. The ECHAM elevation relation gives less elevation change than Dansgaard's, although it has a larger  $\delta^{18}\text{O}$  discrepancy. The reason for this is that the slope of the ECHAM elevation relation is almost double that of Dansgaard's one. For converting  $\delta^{18}\text{O}$  to elevation, the difference in  $\delta^{18}\text{O}$  is divided by that that slope. Consequently, the obtained elevation changed by ECHAM is nearly half of the Dandgaard's one.

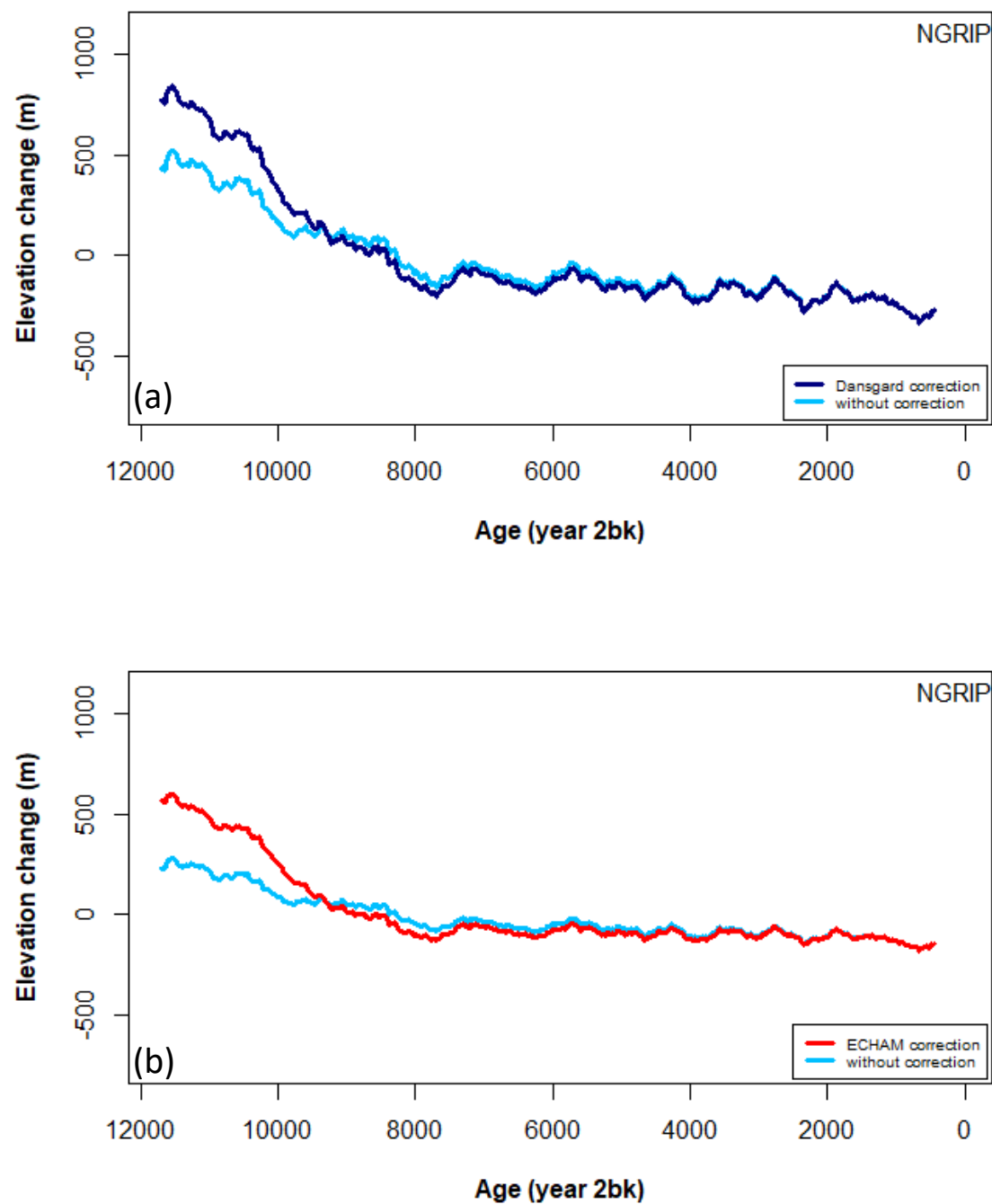


Figure 4.15: NGRIP elevation change relative to the present time based on  $\delta^{18}\text{O}$  difference between Agassiz ice core and NGRIP, by using a) the Dansgaard elevation relation and b) the ECHAM elevation relation.



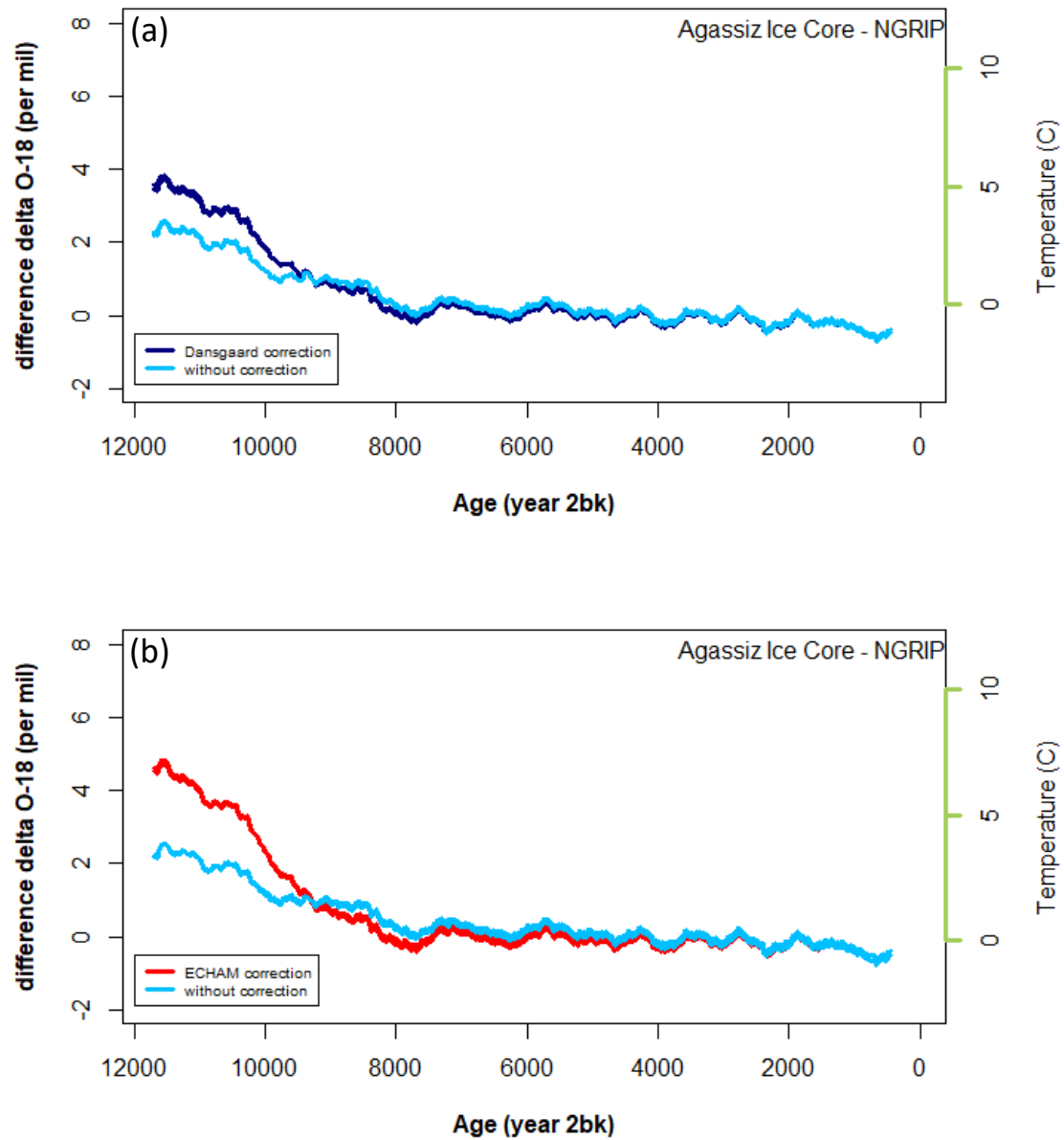


Figure 4.16: Difference of  $\delta^{18}\text{O}$  data and temperature between Agassiz ice core (with and without correction) and NGRIP in Greenland. Converting  $\delta^{18}\text{O}$  to the temperature using a) the Dansgaard temperature relation and b) the ECHAM temperature relation.

### 4.3.2 Non-homogeneous Climate

Another possible assumption is that climate over the Greenland and Ellesmere Island is not homogeneous. In this case, the difference between  $\delta^{18}\text{O}$  records in the two ice caps (Fig. 4.14) is not just due to elevation changes. There is an offset

of 7.7‰ in  $\delta^{18}\text{O}$ , which is due to the peak of Agassiz and NGRIP at different elevations (Fig. 4.14). Fig. 4.16 shows the residual of the temperature variations in the Greenland and Ellesmere Island records over Holocene. The difference between  $\delta^{18}\text{O}$  is higher in the early Holocene (from 12 ka to 8 ka). The Innuitian Ice Sheet retreated over these years (Figs. 4.6 and 4.7). The maximum  $\delta^{18}\text{O}$  difference is 2.17‰, which corresponds to a 2.95 °C and 3.29 °C temperature difference by applying Dansgaard and ECHAM temperature relation, respectively. The elevation correction from the Innuitian Ice Sheet reconstruction increases the discrepancy between the Greenland and Agassiz  $\delta^{18}\text{O}$  (temperature) by 3.40‰ (4.94 °C) and 4.46‰ (6.76 °C) using Dansgaard and ECHAM elevation (temperature) relation, respectively.

## 4.4 Summary

The Innuitian Ice Sheet reconstruction conducted in this thesis has good agreement with RSL constraints (Figs. 4.1 to 4.3). The  $\delta^{18}\text{O}$  correction based on this reconstruction increases the obtained temperature of Agassiz ice cores to 2.14 °C by Dansgaard temperature relation and 3.64 °C using ECHAM temperature relation (Figs. 4.9 to 4.12), which agrees with the results of [Lecavalier et al. \(2017\)](#). This indicates an earlier and warmer Holocene thermal maximum at Agassiz. However, their results show 4-5 °C warmer temperatures compared with their previous temperature reconstruction without correction. They estimated the corrected Agassiz ice core leads to 1 km thinning in Camp Century located in north west of Greenland. I also estimated 755 m and 558 m thinning curve for NGRIP located in centre of Greenland. This value may not be realistic for center of a stable ice sheet like Greenland. However, the temperature difference of 4.94 °C and 6.76 °C based on  $\delta^{18}\text{O}$  difference between NGRIP and corrected Agassiz may not be realistic either. It could also be a result from different factors, such as temporal variation of  $\delta^{18}\text{O}$  to elevation and temperature. The difference between the two ice cores  $\delta^{18}\text{O}$  could be based on the combination of elevation and temperature variation of two sites. So, a reconstruction of the Greenland Ice Sheet could be useful to separate these two

influences in the difference of  $\delta^{18}\text{O}$  between the Greenland and Agassiz Ice Caps.

## Chapter 5

# Conclusion and Outlook

In this thesis a reconstruction of temperature based on  $\delta^{18}\text{O}$  records of the Agassiz ice core and NGRIP were conducted. To do so, the elevation correction should be applied for temperature reconstructions. For this correction I need to determine elevation history of the sites during the Holocene. So, a surface elevation reconstruction is needed in the Agassiz and Devon Ice Caps locations. The ICE-6G reconstruction was initially used as a base reconstruction to show variation of ice thickness and surface elevation after LGM until present time. Subsequently, the Innuitian Ice Sheet was reconstructed with the ICESHEET program written by [Gowan et al. \(2016b,a\)](#). Ice margin, shear stress, and topography are three inputs of ICESHEET program. Relative sea level constraints from Ellesmere and Devon Island were used to evaluate the reconstruction results. The Greenland and Laurentide Ice Sheet were also included in my reconstruction because they influenced the GIA in this region. The Laurentide and Greenland Ice Sheets' margins are based on [Gowan \(2014\)](#) and [Dyke \(2004\)](#), respectively. The margins of the Innuitian Ice Sheet from 22 ka to present are based on [Dyke \(2004\)](#) and [England et al. \(2006\)](#). For advance phase (between 30 ka to 22 ka) the ice sheet margins were reconstructed based on data from [England et al. \(2006\)](#), [England et al. \(2000\)](#), [England \(1999\)](#), and [England et al. \(2004\)](#).

The Devon Ice Cap has constant elevation from 12 ka to present time. Consequently, there is no elevation correction required for its  $\delta^{18}\text{O}$  records. However, the Agassiz

Ice Cap experienced 408 m surface elevation change from 11.7 ka to present time. Dansgaard and Gundestrup (1973)'s relation of  $\delta^{18}\text{O}$  versus temperature are used for correcting  $\delta^{18}\text{O}$ . Additionally, ECHAM-wiso data [Butzin et al., 2014] were used to obtain special  $\delta^{18}\text{O}$  relationship versus temperature and elevation. The early Holocene is warmer when the corrections are applied. The corrected temperatures are 2.14 °C and 3.64 °C for Dansgaard and ECHAM-wiso temperature relation, respectively. The peak temperature happens 500 years earlier in the Agassiz ice cores using the corrections.

The Greenland elevation and temperature changes through the Holocene are reconstructed by taking the difference of  $\delta^{18}\text{O}$  data between the NGRIP and Agassiz ice cores, using two different assumptions. Assuming homogeneous climate over the Northern Canada and Greenland, the elevation changes of NGRIP were estimated (Chapter 4). Using Dansgaard equation, the elevation change is calculated to be 422 m, while the ECHAM equation results in 226 m. The elevation change increases by 334 m and 331 m using the corrected  $\delta^{18}\text{O}$  using Dansgaard and ECHAM corrections. In this method the reconstructed elevation changes of NGRIP is highly dependent on the relation between  $\delta^{18}\text{O}$ -elevation and temperature. Consequently, the uncertainty of calculated elevation is high. Another assumption is non-homogeneous climate in this region, which means the difference between  $\delta^{18}\text{O}$  records of NGRIP and Agassiz is due to a temperature difference. The reconstructed temperature changes with both corrections is conducted. In this case, the original temperature difference at 11.7 ka between the middle of Greenland and Ellesmere Island is about 3 °C. The elevation corrections at the Agassiz Ice Cap increase it to 4.94 °C using Dansgaard's relation and 6.76 °C using ECHAM-wiso.

There are further steps that could be done to improve the climate reconstruction of this region. Reconstruction of the Greenland Ice Sheet with the ICESHEET program could help to assess elevation change of Greenland based on relative sea level. That could be used for evaluating elevation reconstruction using  $\delta^{18}\text{O}$  of ice cores. Improving the Innuitian Ice Sheet by adding RSL constraints of other

regions such as Axel-Heiberg Island could also improve the reconstructed elevation of the Agassiz and Devon Ice Caps. Investigating the relation of  $\delta^{18}\text{O}$ -elevation and temperature during the early Holocene could improve the applied correction. The earlier and warmer maximum temperature could be checked with Sea Surface Temperature (SST) reconstruction.

# Bibliography

- Alley, R., Meese, D., Shuman, C., Gow, A., Taylor, K., Grootes, P., White, J., Ram, M., Waddington, E., Mayewski, P., et al. (1993). Abrupt increase in Greenland snow accumulation at the end of the Younger Dryas event. *Letters of Nature*, pages 1567–1570.
- Alley, R. B., Mayewski, P. A., Sowers, T., Stuiver, M., Taylor, K. C., and Clark, P. U. (1997). Holocene climatic instability: A prominent, widespread event 8200 yr ago. *Geology*, 25(6):483–486.
- Andersen, K. K., Azuma, N., Barnola, J.-M., Bigler, M., Biscaye, P., Caillon, N., Chappellaz, J., Clausen, H. B., Dahl-Jensen, D., Fischer, H., et al. (2004). High-resolution record of Northern Hemisphere climate extending into the last interglacial period. *Nature*, 431(7005):147–151.
- Argus, D. F., Peltier, W., Drummond, R., and Moore, A. W. (2014). The Antarctica component of postglacial rebound model ICE-6G\_C (VM5a) based on GPS positioning, exposure age dating of ice thicknesses, and relative sea level histories. *Geophysical Journal International*, 198(1):537–563.
- Audi, G. and Wapstra, A. (1993). The 1993 atomic mass evaluation:(I) Atomic mass table. *Nuclear Physics A*, 565(1):1–65.
- Audi, G. and Wapstra, A. (1995). The 1995 update to the atomic mass evaluation. *Nuclear Physics A*, 595(4):409–480.
- Bard, E. and Broecker, W. S. (1992). *The Last Deglaciation: Absolute and Radiocarbon Chronologies: [proceedings of the NATO Advanced Research Workshop on Held at Erice]*. Springer-Verlag.
- Barnola, J., Schwander, J., and Staufferl, B. (1993). Synchronous changes in atmospheric CH<sub>4</sub> and Greenland climate between 40 and 8 kyr BP. *Nature*, 366:2.
- Beck, J. W., Richards, D. A., Lawrence, R., Silverman, B. W., Smart, P. L., Donahue, D. J., Herrera-Osterheld, S., Burr, G. S., Calsoyas, L., Timothy, A., et al. (2001). Extremely large variations of atmospheric <sup>14</sup>C concentration during the last glacial period. *Science*, 292(5526):2453–2458.
- Blake Jr, W. (1970). Studies of glacial history in Arctic Canada. I. Pumice, radiocarbon dates, and differential postglacial uplift in the eastern Queen Elizabeth Islands. *Canadian Journal of Earth Sciences*, 7(2):634–664.
- Bowman, S. and Leese, M. (1995). RADIOCARBON CALIBRATION-CURRENT ISSUES. *American Journal of Archaeology*, 99(1):102–105.

- Bradley, R. S. (1999). *Paleoclimatology: reconstructing climates of the Quaternary*, volume 68. Academic Press.
- Brunt, D. (1933). The adiabatic lapse-rate for dry and saturated air. *Quarterly Journal of the Royal Meteorological Society*, 59(252):351–360.
- Butzin, M., Köhler, P., and Lohmann, G. (2017). Marine radiocarbon reservoir age simulations for the past 50,000 years. *Geophysical Research Letters*, 44(16):8473–8480.
- Butzin, M., Werner, M., Masson-Delmotte, V., Risi, C., Frankenberg, C., Gribanov, K., Jouzel, J., and Zakharov, V. I. (2014). Variations of oxygen-18 in West Siberian precipitation during the last 50 years. *Atmospheric Chemistry and Physics*, 14(11):5853–5869.
- Clark, J. A., Farrell, W. E., and Peltier, W. R. (1978). Global changes in postglacial sea level: a numerical calculation. *Quaternary Research*, 9(3):265–287.
- Clausen, H. B. (1973). Dating of polar ice by  $^{32}\text{Si}$ . *Journal of Glaciology*, 12(66):411–416.
- Criss, R. E. (1999). *Principles of stable isotope distribution*. Oxford University Press.
- Cuffey, K. M., Alley, R. B., Grootes, P. M., Bolzan, J. M., and Anandakrishnan, S. (1994). Calibration of the  $\delta^{18}\text{O}$  isotopic paleothermometer for central Greenland, using borehole temperatures. *Journal of Glaciology*, 40(135):341–349.
- Cuffey, K. M., Clow, G. D., Alley, R. B., Stuiver, M., et al. (1995). Large Arctic temperature change at the Wisconsin-Holocene glacial transition. *Science*, 270(5235):455.
- Dahl-Jensen, D., Gundestrup, N. S., Miller, H., Watanabe, O., Johnsen, S. J., Steffensen, J. P., Clausen, H. B., Svensson, A., and Larsen, L. B. (2002). The NorthGRIP deep drilling programme. *Annals of Glaciology*, 35(1):1–4.
- Dansgaard, W., J.-S. J. C. H. B. and Gundestrup, N. (1973). Stable isotope glaciology. on Greenland. (2):1–53.
- Dansgaard, W. (1953). The abundance of O18 in atmospheric water and water vapour. *Tellus*, 5(4):461–469.
- Dansgaard, W. (1954). The O18-abundance in fresh water. *Geochimica et Cosmochimica Acta*, 6(5-6):241–260.
- Dansgaard, W. (1961). The Isotopic Composition of Natural Waters with Seciak Reference to The Greenland Ice Cap. Technical report, Oersted Inst., Copenhagen.
- Dansgaard, W. (1964). Stable isotopes in precipitation. *Tellus*, 16(4):436–468.
- Dansgaard, W., Johnsen, S., Clausen, H., Hvidberg, C., and Steffensen, J. (1993). Evidence for general instability of past climate from a 250-kyr. *Nature*, 364:15.
- Dyke, A. S. (1998). Holocene delevelling of Devon Island, Arctic Canada: implications for ice sheet geometry and crustal response. *Canadian Journal of Earth Sciences*, 35(8):885–904.
- Dyke, A. S. (2004). An outline of North American deglaciation with emphasis on central and northern Canada. *Developments in Quaternary Sciences*, 2:373–424.



- Dziwonski, A. M. and Anderson, D. L. (1981). Preliminary reference Earth model. *Physics of the earth and planetary interiors*, 25(4):297–356.
- England, J. (1990). The late Quaternary history of Greely Fiord and its tributaries, west-central Ellesmere Island. *Canadian Journal of Earth Sciences*, 27(2):255–270.
- England, J. (1996). Glacier dynamics and paleoclimatic change during the last glaciation of eastern Ellesmere Island, Canada. *Canadian Journal of Earth Sciences*, 33(5):779–799.
- England, J. (1999). Coalescent Greenland and Innuitian ice during the last glacial maximum: revising the Quaternary of the Canadian High Arctic. *Quaternary Science Reviews*, 18(3):421–456.
- England, J., Atkinson, N., Bednarski, J., Dyke, A., Hodgson, D., and Cofaigh, C. Ó. (2006). The Innuitian Ice Sheet: configuration, dynamics and chronology. *Quaternary Science Reviews*, 25(7):689–703.
- England, J., Dyke, A. S., Coulthard, R. D., Mcneely, R., and Aitken, A. (2013). The exaggerated radiocarbon age of deposit-feeding molluscs in calcareous environments. *Boreas*, 42(2):362–373.
- England, J., Smith, I. R., and Evans, D. J. (2000). The last glaciation of east-central Ellesmere Island, Nunavut: ice dynamics, deglacial chronology, and sea level change. *Canadian Journal of Earth Sciences*, 37(10):1355–1371.
- England, J. H., Atkinson, N., Dyke, A. S., Evans, D. J., and Zreda, M. (2004). Late wisconsinan buildup and wastage of the innuitian Ice Sheet across southern Ellesmere Island, Nunavut. *Canadian Journal of Earth Sciences*, 41(1):39–61.
- Epstein, S. (1959). The variations of the  $18\text{O}/16\text{O}$  ratios in nature and some geologic implications. *Researches in Geochemistry*. Wiley, New York, pages 217–240.
- Farrell, W. and Clark, J. A. (1976). On postglacial sea level. *Geophysical Journal International*, 46(3):647–667.
- Fisher, D. (1976). *A study of two O-18 records from Devon Ice cap, Canada, and comparison of them to Camp Century O-18 record, Greenland*. PhD thesis, University of Copenhagen.
- Fisher, D. and Koerner, R. (1981). Some aspects of climatic change in the High Arctic during the Holocene as deduced from ice cores. *W. Maheney, Geology Abstracts*, pages 249–271.
- Fisher, D., Koerner, R., Paterson, W., Dansgaard, W., Gundestrup, N., and Reeh, N. (1983). Effect of wind scouring on climatic records from ice-core oxygen-isotope profiles. *Nature*, 301:205–209.
- Fisher, D., Reeh, N., and Langley, K. (1985). Objective reconstructions of the Late Wisconsinan Laurentide Ice Sheet and the significance of deformable beds. *Géographie physique et Quaternaire*, 39(3):229–238.
- Fisher, D., Zheng, J., Burgess, D., Zdanowicz, C., Kinnard, C., Sharp, M., and Bourgeois, J. (2012). Recent melt rates of Canadian arctic ice caps are the highest in four millennia. *Global and Planetary Change*, 84:3–7.

- Fisher, D. A. (1979). Comparison of 105 years of oxygen isotope and insoluble impurity profiles from the Devon Island and Camp Century ice cores. *Quaternary Research*, 11(3):299–305.
- Fisher, D. A., Koerner, R. M., and Reeh, N. (1995). Holocene climatic records from Agassiz ice cap, Ellesmere Island, NWT, Canada. *The Holocene*, 5(1):19–24.
- Forte, A. M. and Mitrovica, J. X. (2001). Deep-mantle high-viscosity flow and thermochemical structure inferred from seismic and geodynamic data. *Nature*, 410(6832):1049–1056.
- Godwin, H. and Willis, E. (1961). Cambridge University natural radiocarbon measurements III. *Radiocarbon*, 3(1):60–76.
- Gowan, E. (2014). *Model of the western Laurentide Ice Sheet, North America*. PhD thesis, PhD thesis, The Australian National University, Canberra, ACT, Australia.
- Gowan, E. J. (2013). An assessment of the minimum timing of ice free conditions of the western Laurentide Ice Sheet. *Quaternary Science Reviews*, 75:100–113.
- Gowan, E. J., Fransner, O. J., and Dowdeswell, J. (2016a). ICESHEET 1.0: a program to produce paleo-ice sheet reconstructions with minimal assumptions. *Geoscientific Model Development*, 9(5):1673.
- Gowan, E. J., Tregoning, P., Purcell, A., Montillet, J.-P., and McClusky, S. (2016b). A model of the western Laurentide Ice Sheet, using observations of glacial isostatic adjustment. *Quaternary Science Reviews*, 139:1–16.
- Hammer, C., Clausen, H., Dansgaard, W., Gundestrup, N., Johnsen, S., and Reeh, N. (1978). Dating of Greenland ice cores by flow models, isotopes, volcanic debris, and continental dust. *Journal of Glaciology*, 20(82):3–26.
- Hansen, B. L. and Langway Jr, C. (1966). Deep core drilling in ice and core analysis at Camp Century, Greenland, 1961-1966. *Antarctic Journal of the United States*, 1(5):207–08.
- Hughen, K. A., Overpeck, J. T., Peterson, L. C., and Trumbore, S. (1996). Rapid climate changes in the tropical Atlantic region during the last deglaciation. *Nature*, 380(6569):51.
- Imbrie, J., Boyle, E., Clemens, S., Duffy, A., Howard, W., Kukla, G., Kutzbach, J., Martinson, D., McIntyre, A., Mix, A., et al. (1992). On the structure and origin of major glaciation cycles 1. Linear responses to Milankovitch forcing. *Paleoceanography*, 7(6):701–738.
- James, T. S., Gowan, E. J., Wada, I., and Wang, K. (2009). Viscosity of the asthenosphere from glacial isostatic adjustment and subduction dynamics at the northern Cascadia subduction zone, British Columbia, Canada. *Journal of Geophysical Research: Solid Earth*, 114(B4).
- Johnsen, S., Clausen, H., Dansgaard, W., Fuhrert, K., Gundestrup, N., Hammer, C., Iversen, P., Jouzel, I., and Stauffer, B. (1992a). Irregular glacial interstadials, recorded in a new Greenland. *Nature*, 3:24.

- Johnsen, S., Dansgaard, W., and White, J. (1989). The origin of Arctic precipitation under present and glacial conditions. *Tellus B*, 41(4):452–468.
- Johnsen, S. J., Clausen, H. B., Dansgaard, W., Gundestrup, N. S., Hansson, M., Jonsson, P., Steffensen, J. P., and Sveinbjörnsdóttir, A. E. (1992b). A "deep" ice core from East Greenland. *MoG Geoscience*, 29.
- Johnsen, S. J., Dahl-Jensen, D., Gundestrup, N., Steffensen, J. P., Clausen, H. B., Miller, H., Masson-Delmotte, V., Sveinbjörnsdóttir, A. E., and White, J. (2001). Oxygen isotope and palaeotemperature records from six Greenland ice-core stations: Camp Century, Dye-3, GRIP, GISP2, Renland and NorthGRIP. *Journal of Quaternary Science*, 16(4):299–307.
- Kerney, M. P., Levy, J., and Oakley, K. (1963). Late-glacial deposits on the Chalk of south-east England. *Philosophical Transactions of the Royal Society of London B: Biological Sciences*, 246(730):203–254.
- Kittel, C. and Kroemer, H. (1980). *Thermal Physics*. Macmillan.
- Koerner, R. and Fisher, D. (1981). Studying climatic change from Canadian high Arctic ice cores. *Climatic change in Canada*, 2:195–218.
- Koerner, R. and Fisher, D. (1990). A record of Holocene summer climate from a Canadian high-Arctic ice core. *Nature*, 343(6259):630–631.
- Laj, C., Mazaud, A., and Duplessy, J.-C. (1996). Geomagnetic intensity and  $^{14}\text{C}$  abundance in the atmosphere and ocean during the past 50 kyr. *Geophysical Research Letters*, 23(16):2045–2048.
- Lambeck, K., Purcell, A., and Zhao, S. (2017). The North American Late Wisconsin ice sheet and mantle viscosity from glacial rebound analyses. *Quaternary Science Reviews*, 158:172–210.
- Lecavalier, B. S., Fisher, D. A., Milne, G. A., Vinther, B. M., Tarasov, L., Huybrechts, P., Lacelle, D., Main, B., Zheng, J., Bourgeois, J., et al. (2017). High Arctic Holocene temperature record from the Agassiz ice cap and Greenland ice sheet evolution. *Proceedings of the National Academy of Sciences*, 114(23):5952–5957.
- Libby, W. F. (1952). Chicago radiocarbon dates, III. *Science*, 116(3025):673–681.
- Mayewski, P. A., Meeker, L. D., Whitlow, S., Twickler, M. S., Morrison, M. C., Alley, R. B., Bloomfield, P., and Taylor, K. (1993). The atmosphere during the Younger Dryas. *Science*, 261(5118):195–198.
- Mazaud, A., Laj, C., Bard, E., Arnold, M., and Tric, E. (1991). Geomagnetic field control of  $^{14}\text{C}$  production over the last 80 Ky: Implications for the radiocarbon time-scale. *Geophysical Research Letters*, 18(10):1885–1888.
- Milankovitch, M. (1930). Mathematische klimalehre und astronomische theorie der klimaschwankungen. *Handbuch der Klimatologie*, 1.
- Milne, G. A., Mitrovica, J. X., and Schrag, D. P. (2002). Estimating past continental ice volume from sea-level data. *Quaternary Science Reviews*, 21(1):361–376.

- Nakada, M., Okuno, J., and Irie, Y. (2017). Inference of viscosity jump at 670 km depth and lower-mantle viscosity structure from GIA observations. *Geophysical Journal International*.
- National Oceanic and Atmospheric Administration. Ice Core Data By Location. <https://www.ncdc.noaa.gov/cdo/f?p=535:9:0:::~:~:~:~:m>.
- Nye, J. (1952). A method of calculating the thicknesses of the ice-sheets. *Nature*, 169:529–530.
- Oeschger, H., Stauffer, P., Bucher, P., and Moell, M. (1976). Instruments and Methods Extraction of Trace Components from Large Quantities of Ice In Bore Holes: Extraction of Trace Components from Large Quantities of Ice In Bore. *Journal of Glaciology*, 17(75):117–128.
- Panasjuk, S. V. and Hager, B. H. (2000). Inversion for mantle viscosity profiles constrained by dynamic topography and the geoid, and their estimated errors. *Geophysical Journal International*, 143(3):821–836.
- Paterson, W., Koerner, R., Fisher, D., Johnsen, S., Clausen, H., Dansgaard, W., Bucher, P., and Oeschger, H. (1977). An oxygen-isotope climatic record from the Devon Island Ice Cap, Arctic Canada.
- Peltier, W. (1974). The impulse response of a Maxwell Earth. *Reviews of Geophysics*, 12(4):649–669.
- Peltier, W. (1976). Glacial-isostatic adjustment-II. The inverse problem. *Geophysical Journal International*, 46(3):669–705.
- Peltier, W. and Andrews, J. (1976). Glacial-isostatic adjustment-I. The forward problem. *Geophysical Journal International*, 46(3):605–646.
- Peltier, W., Argus, D., and Drummond, R. (2015). Space geodesy constrains ice age terminal deglaciation: The global ICE-6G\_C (VM5a) model. *Journal of Geophysical Research: Solid Earth*, 120(1):450–487.
- Peltier, W., Farrell, W., and Clark, J. (1978). Glacial isostasy and relative sea level: a global finite element model. *Tectonophysics*, 50(2-3):81–110.
- Prest, V. (1969). Retreat of wisconsin and recent ice in north america: Canada geol. *Survey Map*, 1257.
- Ramsey, C. B. (1995). Radiocarbon calibration and analysis of stratigraphy: the OxCal program. *Radiocarbon*, 37(02):425–430.
- Ramsey, C. B. (2009). Bayesian analysis of radiocarbon dates. *Radiocarbon*, 51(1):337–360.
- Rasmussen, S. O., Andersen, K. K., Svensson, A., Steffensen, J. P., Vinther, B. M., Clausen, H. B., Siggaard-Andersen, M.-L., Johnsen, S. J., Larsen, L. B., Dahl-Jensen, D., et al. (2006). A new Greenland ice core chronology for the last glacial termination. *Journal of Geophysical Research: Atmospheres*, 111(D6).
- Reeh, N. (1982). A plasticity theory approach to the steady-state shape of a three-dimensional ice sheet. *Journal of Glaciology*, 28(100):431–455.

- Reimer, P. J., Bard, E., Bayliss, A., Beck, J. W., Blackwell, P. G., Ramsey, C. B., Buck, C. E., Cheng, H., Edwards, R., Lawrence, and Michael, F. (2013). IntCal13 and Marine13 radiocarbon age calibration curves 0–50,000 years cal BP. *Radiocarbon*, 55(4):1869–1887.
- Renssen, H., Goosse, H., Fichefet, T., and Campin, J. (2001). The 8.2 kyr BP event simulated by a global atmosphere sea ice ocean model. *Geophysical Research Letters*, 28(8):1567–1570.
- Robin, G. d. Q. (2010). *The climatic record in polar ice sheets*. Cambridge University Press.
- Rosman, K. and Taylor, P. (1998). Isotopic compositions of the elements 1997 (Technical Report). *Pure and Applied Chemistry*, 70(1):217–235.
- Schaffer, J., Timmermann, R., Arndt, J. E., Kristensen, S. S., Mayer, C., Morlighem, M., and Steinhage, D. (2016). A global, high-resolution data set of ice sheet topography, cavity geometry, and ocean bathymetry. *Earth System Science Data*, 8(2):543.
- Sella, G. F., Stein, S., Dixon, T. H., Craymer, M., James, T. S., Mazzotti, S., and Dokka, R. K. (2007). Observation of glacial isostatic adjustment in stable North America with GPS. *Geophysical Research Letters*, 34(2).
- Sinpetru, L. It Rained Buckets of Iron on Young Earth, New Study Finds. <http://news.softpedia.com/news/It-Rained-Buckets-of-Iron-on-Young-Earth-New-Study-Finds-476189.shtml>, lastchecked = 2017-03-09, originalyear = 2015.
- Steinberger, B. and Calderwood, A. R. (2006). Models of large-scale viscous flow in the Earth’s mantle with constraints from mineral physics and surface observations. *Geophysical Journal International*, 167(3):1461–1481.
- Stone, P. H. and Carlson, J. H. (1979). Atmospheric lapse rate regimes and their parameterization. *Journal of the Atmospheric Sciences*, 36(3):415–423.
- Stuiver, M. and Reimer, P. J. (1993). Extended 14 C data base and revised CALIB 3.0 14 C age calibration program. *Radiocarbon*, 35(01):215–230.
- Tzedakis, P., Andrieu, V., De Beaulieu, J.-L., Crowhurst, S. d., Follieri, M., Hooghiemstra, H., Magri, D., Reille, M., Sadori, L., and Shackleton, N. (1997). Comparison of terrestrial and marine records of changing climate of the last 500,000 years. *Earth and Planetary Science Letters*, 150(1-2):171–176.
- Valkovic, V. (2000). *Radioactivity in the Environment: Physicochemical aspects and applications*. Elsevier.
- Vinther, B. M., Buchardt, S. L., Clausen, H. B., Dahl-Jensen, D., Johnsen, S. J., Fisher, D., Koerner, R., Raynaud, D., Lipenkov, V., and Andersen, K. (2009). Holocene thinning of the Greenland ice sheet. *Nature*, 461(7262):385–388.
- Vinther, B. M., Clausen, H. B., Fisher, D., Koerner, R., Johnsen, S. J., Andersen, K. K., Dahl-Jensen, D., Rasmussen, S. O., Steffensen, J. P., and Svensson, A. (2008). Synchronizing ice cores from the Renland and Agassiz ice caps to the Greenland Ice Core Chronology. *Journal of Geophysical Research: Atmospheres*, 113(D8).

- Vinther, B. M., Clausen, H. B., Johnsen, S. J., Rasmussen, S. O., Andersen, K. K., Buchardt, S. L., Dahl-Jensen, D., Seierstad, I. K., Siggaard-Andersen, M.-L., and Steffensen, J. P. (2006). A synchronized dating of three Greenland ice cores throughout the Holocene. *Journal of Geophysical Research: Atmospheres*, 111(D13).
- Voelker, A. H., Grootes, P. M., Nadeau, M.-J., and Sarnthein, M. (2000). Radiocarbon levels in the Iceland Sea from 25–53 kyr and their link to the Earth’s magnetic field intensity. *Radiocarbon*, 42(3):437–452.
- Wallace, J. M. and Hobbs, P. V. (2006). *Atmospheric science: an introductory survey*, volume 92. Academic press.
- Werner, M., Langebroek, P., Carlsen, T., Herold, M., and Lohmann, G. (2011). Stable water isotopes in the ECHAM5 general circulation model: Towards high-resolution isotope modeling on a global scale. *Journal of Geophysical Research - Atmospheres*, 116, D15109.
- Zheng, J., Kudo, A., Fisher, D. A., Blake, E. W., and Gerasimoff, M. (1998). Solid electrical conductivity (ECM) from four Agassiz ice cores, Ellesmere Island NWT, Canada: High-resolution signal and noise over the last millennium and low resolution over the Holocene. *The Holocene*, 8(4):413–421.